Pheromone-induced morphogenesis and gradient tracking are dependent on the MAPK Fus3 binding to Gα

Beverly Errede[a], Lior Vered[b], Eintou Ford[a,*], Matthew I. Pena[a,†], and Timothy C. Elston[c]
[a]Department of Biochemistry and Biophysics, [b]Department of Chemistry, and [c]Department of Pharmacology, University of North Carolina, Chapel Hill, NC 27599

ABSTRACT **Mitogen-activated protein kinase (MAPK) pathways control many cellular processes, including differentiation and proliferation. These pathways commonly activate MAPK isoforms that have redundant or overlapping function. However, recent studies have revealed circumstances in which MAPK isoforms have specialized, nonoverlapping roles in differentiation. The mechanisms that underlie this specialization are not well understood. To address this question, we sought to establish regulatory mechanisms that are unique to the MAPK Fus3 in pheromone-induced mating and chemotropic fate transitions of the budding yeast *Saccharomyces cerevisiae*. Our investigations reveal a previously unappreciated role for inactive Fus3 as a potent negative regulator of pheromone-induced chemotropism. We show that this inhibitory role is dependent on inactive Fus3 binding to the α-subunit of the heterotrimeric G-protein. Further analysis revealed that the binding of catalytically active Fus3 to the G-protein is required for gradient tracking and serves to suppress cell-to-cell variability between mating and chemotropic fates in a population of pheromone-responding cells.**

Monitoring Editor
Charles Boone
University of Toronto

Received: Mar 26, 2015
Revised: Jun 25, 2015
Accepted: Jul 8, 2015

INTRODUCTION

Cell fate decisions are mediated by growth factors that signal through mitogen-activated protein kinase (MAPK) pathways (Corson *et al.*, 2003; Shilo, 2003, 2005). Depending on context, the same growth factor either induces or inhibits the ability of a cell to differentiate. In unicellular organisms such as budding yeast (*Saccharomyces cerevisiae*), mating pheromone specifies two alternative cell fates that are dependent on stimulus dosage (Figure 1). Haploid **a** and α cells in proximity to each other respond to the localized high dose of pheromone secreted by the opposite cell type (Schrick *et al.*, 1997). Cells arrest in the G1 phase of the cell cycle and polarize their growth to form a specialized structure called a mating projection or "shmoo," which is the site of contact and fusion between mating partners. When haploid cells are exposed to lower doses of pheromone, they transiently arrest in the G1 phase of the cell cycle and exhibit hyperpolarized growth that gives the cells an elongated, worm-like morphology. As cells reenter the cell cycle, they exhibit a polar rather than an axial budding pattern (Erdman and Snyder, 2001). We call this cell type "chemotropic" because growth is hyperpolarized in the direction of increasing pheromone concentration (Segall, 1993; Paliwal *et al.*, 2007; Hao *et al.*, 2008).

The developmental programs leading to either pheromone-induced mating differentiation or chemotropic growth depend on the identical signaling pathway (Figure 1; Dohlman and Thorner, 2001; Erdman and Snyder, 2001). This pathway is activated when peptide pheromone secreted by one cell type binds to its G-protein–coupled receptor in cells of the opposite cell type (α-factor to Ste2 in **a** cells or **a**-factor to Ste3 in α cells). The pheromone–receptor complex activates a heterotrimeric G-protein (Gα-Gpa1/Gβ-Ste4/Gγ-Ste18), which propagates the signal by activating a MAPK cascade. The scaffold-Ste5 organizes the core enzymes of the MAPK cascade by binding directly to the MAPKKK-Ste11, the MAPKK-Ste7, and the MAPK-Fus3. The MAPK-Kss1 is

This article was published online ahead of print in MBoC in Press (http://www.molbiolcell.org/cgi/doi/10.1091/mbc.E15-03-0176) on July 15, 2015.

Present addresses: *Department of Pharmacy, Campbell University, Buies Creek, NC 27506; †Department of BioSciences, Rice University, Houston, TX 77251.

Address correspondence to: B. Errede (errede@email.unc.edu).

Abbreviations used: α-fr, alpha-factor (pheromone); AU, arbitrary units; CTM, carboxy-terminal trans membrane; DIC, differential interference contrast; FDG, fluorescein di(β-D-galactopyranoside); G6PDH, glucose-6-phosphate dehydrogenase; HRP, horseradish peroxidase; IgG, immunoglobulin G; MAPK, mitogen-activated protein kinase; MAPKK, mitogen-activated protein kinase kinase; MAPKKK, mitogen-activated protein kinase kinase kinase; OD, optical density; PRE, pheromone response element; SCF, Skp1/Cul1/F-box complex; TCS, Tec1 consensus binding sequence.

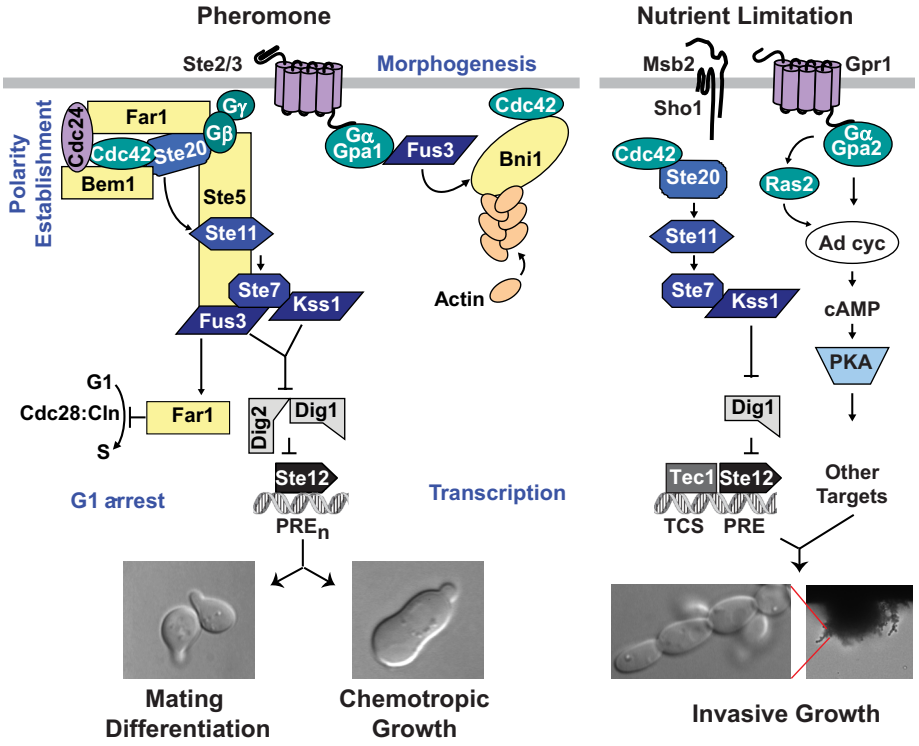

FIGURE 1: Signal transduction pathways controlling pheromone-induced responses and nutrient limitation–induced invasive growth. See the text for explanation.

part of the complex through its binding interaction with the MAPKK-Ste7. The scaffold-Ste5 also binds to Gβ-Ste4, and this interaction serves to colocalize the assembly with the p20-activated kinase (PAK) Ste20 (Whiteway *et al.*, 1995; Leeuw *et al.*, 1998). PAK-Ste20 functions in the MAPK module by phosphorylating and activating the MAPKKK-Ste11 (Wu *et al.*, 1995; van Drogen *et al.*, 2000).

In addition to mating projection formation and chemotropism, haploid yeast undergo a distinct transition from a vegetative to a pseudofilamentous polarized growth mode on rich medium in response to glucose depletion or high alcohol (for review, see Palecek *et al.*, 2002; Truckses *et al.*, 2004). Cells emerging from the periphery of colonies under these nutrient-limited conditions invade the substratum and form chains of highly elongated cells, resulting in an invasive growth phenotype. This transition requires the integration of MAPK and protein kinase A (PKA)–mediated responses. With the exception of the receptors, G-protein, Fus3, and Ste5, the MAPK branch of the network has the same signaling components as the pheromone response pathway (Figure 1; Liu *et al.*, 1993; Roberts and Fink, 1994).

Strains with different single or double deletions of *FUS3* and *KSS1* exhibit differences in their ability to differentiate, revealing specialized roles for the two MAPKs in the mating and filamentous growth programs (Breitkreutz and Tyers, 2002). Both Fus3 and Kss1 promote pheromone-induced transcription (Roberts *et al.*, 2000; Breitkreutz *et al.*, 2001). However, active Fus3 has a predominant role in mating differentiation, as most laboratory strains have more severe mating defects in *fus3*Δ than in *kss1*Δ mutants (Elion *et al.*, 1991). This principal role is attributed to phosphoproteins essential for mating that are preferential substrates for Fus3 rather than Kss1 (Farley *et al.*, 1999; Breitkreutz *et al.*, 2001). For example, Fus3 more efficiently phosphorylates Far1 than does Kss1. This phosphorylation promotes Far1 function as a Cdc28-cyclin inhibitor and polarity complex scaffold during the mating response (Peter *et al.*, 1993; Butty *et al.*, 1998; Blondel *et al.*, 1999; Shimada *et al.*, 2000). In addition, Fus3 binding to Gα-Gpa1 and phosphorylation of Bni1 facilitates pheromone-induced morphogenesis (Metodiev *et al.*, 2002; Matheos *et al.*, 2004). Active Kss1 is believed to be the principal MAPK required for promoting nutrient-regulated filamentous growth, whereas active Fus3 has an inhibitory role. This interpretation stems from the observation that haploid *kss1*Δ strains are not invasive, whereas *fus3*Δ strains invade more robustly than wild-type strains (Cook *et al.*, 1997; Breitkreutz *et al.*, 2003). Although the roles of Fus3 and Kss1 in the chemotropic program are less well understood, both have a positive regulatory role. Strains with a single *kss1*Δ or *fus3*Δ mutation are fully competent to hyperpolarize their growth and switch to a polar budding pattern, whereas *fus3*Δ *kss1*Δ double-mutant strains are completely defective (Erdman and Snyder, 2001). Again, Fus3 has additional roles in this developmental program that are not shared with Kss1. First, *fus3*Δ strains are defective in directing hyperpolarized growth toward increasing pheromone concentration (gradient tracking; Hao *et al.*, 2008). Second, *fus3*Δ strains fail to restrict hyperelongation to conditions of low pheromone concentrations (Esch *et al.*, 2006; Hao *et al.*, 2008).

Although the three morphology transitions described in the foregoing are mediated in whole or in part by the signaling cascade dependent on the MAPKK-Ste7 and the transcription factor Ste12, the developmental outcome depends on whether Fus3, Kss1, or both are active. Specifically, Fus3 but not Kss1 is required for proper shmoo formation (Farley *et al.*, 1999; Matheos *et al.*, 2004) and gradient tracking (Hao *et al.*, 2008), whereas Kss1 appears to be required for cells to respond properly to low pheromone concentration (Paliwal *et al.*, 2007; Hao *et al.*, 2008) and nutrient limitation (Cook *et al.*, 1997; Breitkreutz *et al.*, 2003). Similarly, mammalian Erk1 and Erk2 are MAPK isoforms that are coactivated by different stimuli, but it is becoming increasingly apparent that these isoforms have specialized roles in determining developmental fates (Sarbassov *et al.*, 1997; Fischer *et al.*, 2005; Shin *et al.*, 2010; He *et al.*, 2011; Chang *et al.*, 2012). The mechanisms that underlie these differences among MAPK isoforms have not been fully established. To address this issue, we compared the pheromone-induced responses of transcription, G1 arrest, and morphogenesis under conditions in which Kss1 is active either in the absence of Fus3 (*fus3*Δ) or the presence of a Fus3 variant that is inactive because it cannot be phosphorylated (*fus3A*^{180}*F*^{182}; Gartner *et al.*, 1992). We found that the cells responded differently, depending on whether they lacked Fus3 completely or expressed the Fus3 variant. Further investigation of the phenotypic differences allowed us to distinguish Fus3-specific roles in the pheromone response and furthered our understanding of why chemotropism is repressed under conditions in which Kss1 but not Fus3 is active.

RESULTS

Pheromone responses are more defective in strains expressing nonactivatable Fus3 than in strains completely lacking Fus3

We previously observed that cells undergo invasive growth but are inhibited for pheromone-induced mating differentiation under

Reporter gene		β-Galactosidase activity (AU/min OD_{660})		
PRE_3-LacZ	Pheromone	*FUS3*	*fus3Δ*	*fus3A^{180}F^{182}*
	100 nM	1374 ± 78	1051 ± 125	175 ± 23
	No pheromone	62 ± 5	50 ± 10	16 ± 1
TCS-PRE-LacZ	Pheromone	*FUS3*	*fus3Δ*	*fus3A^{180}F^{182}*
	100 nM	148 ± 12	1153 ± 28	1016 ± 45
	No pheromone	30 ± 6	707 ± 30	544 ± 36
PRE_3-LacZ	Galactose	*P_{GAL1}STE5CTM FUS3*	*P_{GAL1}STE5CTM fus3Δ*	*P_{GAL1}STE5CTM fus3A^{180}F^{182}*
	2%	643 ± 17	43 ± 8	6 ± 1
	No galactose	1 ± 0. 1	1 ± 0. 2	1 ± 0. 3

TABLE 1: Comparison of reporter gene expression in strains with different *FUS3* alleles.

conditions in which Ste7 activates Kss1 but does not activate Fus3 (Maleri *et al.*, 2004). Our interpretation is that under such conditions, inactive Fus3 is present and has a role in the inhibition of mating differentiation. This inhibitory function could serve to ensure against an inappropriate differentiation response, for example, by prevent mating differentiation under nutrient limiting conditions in which Kss1 is active but Fus3 is not. This inhibition could impinge not only on mating differentiation but also on chemotropic growth through mechanisms that affect one or more processes, including transcription, G1 arrest, and polarization. To assess more directly what role(s) inactive Fus3 plays in protecting against inappropriate fate transitions, we generated isogenic strains with wild-type Fus3 (*FUS3*), no Fus3 (*fus3Δ*), or a nonactivatable Fus3 variant (*fus3A^{180}F^{182}*) expressed from the endogenous locus.

To examine the effects of nonactivatable Fus3 on transcription of mating and filamentation gene expression, we measured expression of reporter genes representative of the two transcriptional programs. Consistent with previous observations, the absence of Fus3 (*fus3Δ*) has little effect on pheromone-induced expression of the prototypical mating-specific *PRE_3-lacZ* reporter (Table 1; Roberts *et al.*, 2000; Breitkreutz *et al.*, 2001). In contrast, the strain expressing nonactivatable Fus3 (*fus3A^{180}F^{182}*) shows reduced basal expression and remains at nearly baseline *PRE_3-lacZ* expression after exposure to pheromone. Although Breitkreutz *et al.* (2001) reported that catalytically inert versions of Fus3 altered neither the pheromone-induced transcriptional profile nor the basal level of pheromone induced genes, the data in the supplement they provided are qualitatively consistent with our findings. We suggest that the mechanism of repression of the mating-specific program by Fus3A^{180}F^{182} is analogous to the role inactive Kss1 plays in the inhibition of genes required for the filamentation program (Cook *et al.*, 1997; Madhani *et al.*, 1997; Tedford *et al.*, 1997; Bardwell *et al.*, 1998a; Chou *et al.*, 2006). As previously reported, basal and pheromone-induced expression of the prototypical filamentation-specific *TCS-PRE-lacZ* reporter is significantly elevated (three to four times) in *fus3Δ* and *fus3A^{180}F^{182}* strains compared with the reference *FUS3* strain (Table 1; Madhani *et al.*, 1997; Sabbagh *et al.*, 2001). Thus, in contrast to mating-specific gene expression, Kss1-promoted filamentation specific gene expression is the same in strains without Fus3 or with nonactivatable Fus3 (Table 1).

To compare morphological transitions characteristic of pheromone-induced fates in strains with different *FUS3* alleles, we used microfluidic chambers to expose cells to a pheromone gradient (5–50 nM) over a 5-h time course. Morphological transitions that occur in these gradients depend on pheromone dosage (position in the gradient), time of exposure, and *FUS3* genotype. Cells were placed into one of three morphological categories that are characteristic of different cell types: vegetative (no morphological response to pheromone), shmoo (mating competent), or hyperelongated (chemotropic or filamentous; Figure 2D). The vegetative category includes cells with round or oval shape (whether budded or unbudded). The shmoo category includes unbudded cells with one or more tight projections. The hyperelongated category includes G1-arrested cells with an elongated or peanut shape and mitotic cells in which the buds are hyperelongated (whether the mother has an elongated or round shape).

Before establishing the pheromone gradient, all strains have a round or oval morphology characteristic of vegetative cells. After 5 h in the pheromone gradient, shmoo, hyperelongated, and vegetative morphologies are observed for the wild-type reference cells (*FUS3*), which are largely confined to zones of the microfluidic chamber corresponding to high, intermediate, and low pheromone concentrations, respectively (Hao *et al.*, 2008; Figure 2A). Cells lacking Fus3 (*fus3Δ*) do not shmoo. Instead, they exhibit hyperelongated and vegetative morphologies in all zones of the chamber, a behavior consistent with a prior report (Hao *et al.*, 2008; Figure 2B). Cells expressing nonactivatable Fus3 (*fus3A^{180}F^{182}*) have significantly fewer elongated cells than those without Fus3 (*fus3Δ*) and remain largely in the vegetative growth phase in all zones of the chamber (Figure 2C). The same phenotype was observed with an independently constructed *fus3A^{180}F^{182}* strain (C699-192; unpublished data). The contrasting behaviors of cells without Fus3 and those that express the Fus3 variant show that nonactivatable Fus3 is an inhibitor of morphogenesis characteristic of chemotropic cells.

In addition to activating pheromone-specific transcription, Fus3 promotes cell cycle arrest in G1 by phosphorylating Far1. Therefore, in the same microfluidic experiments, we compared efficiency of the G1 arrest response to pheromone based on the accumulation of unbudded cells in the chamber. Before loading cells into the chamber, all strains had an unbudded cell index (35–45%) characteristic of log-phase cultures in synthetic medium. The initial unbudded cell percentage reported for these microfluidic experiments is slightly higher (45–55%) because the geometry of the chamber causes a slight bias toward loading unbudded G1 cells. After 2 h in the pheromone gradient, >90% of the wild-type reference cells (*FUS3*) in the high– and intermediate–pheromone concentration zones of the gradient were unbudded and remained arrested throughout the remainder of the time course. In the low–pheromone concentration zone, only ~75% of the cells were unbudded, and most of these reentered the cell cycle during the remainder of the time course (Figure 3A). Cells lacking Fus3 (*fus3Δ*) show a less-homogeneous G1

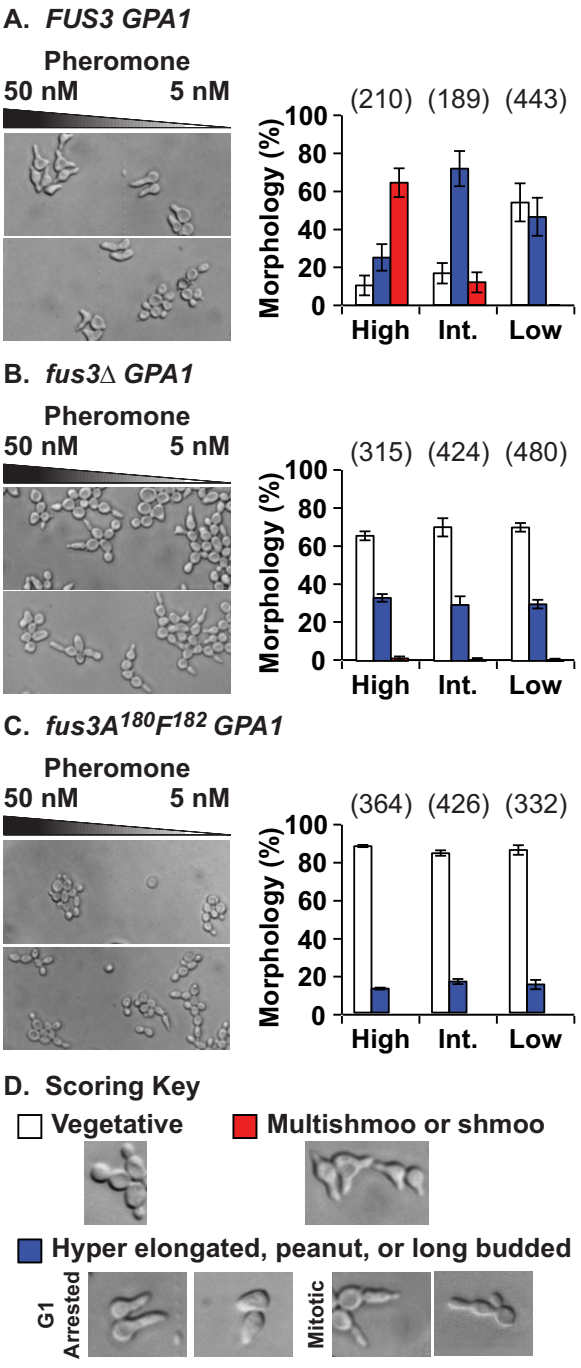

FIGURE 2: Developmental fate morphologies of strains with different *FUS3* alleles in pheromone gradients. Cells from *bar1Δ* strains with *FUS3* (C699-5), *fus3Δ* (C699-200), or *fus3A*^{180}*F*^{182} (C699-207) as indicated, were exposed to a linear gradient of pheromone (50–5 nM) in microfluidic chambers. (A–C) Left, micrographs showing representative fields of cells with the indicated *FUS3* alleles after 5 h of growth in pheromone gradient. Right, bar graphs showing the percentage of cells in the upper (High), intermediate (Int), or lower (Low) one-third of the gradient with vegetative (□), hyperelongated (■), or shmoo (■) morphology after 5 h of exposure to pheromone. Error bars show the 95% confidence limit using data from three or more gradient chamber experiments. The total number of cells scored in each portion of the gradient is given above the bars. (D) Micrographs of cells illustrating representative morphologies for the following scoring categories: vegetative, cells with a round or oval shape (whether budded or unbudded); shmoo, G1 (unbudded) cells with one or more pointed projections; hyperelongated, G1 (unbudded) cells with an elongated or peanut shape and mitotic cells (budded) with a hyperelongated shape and/or hyperelongated bud.

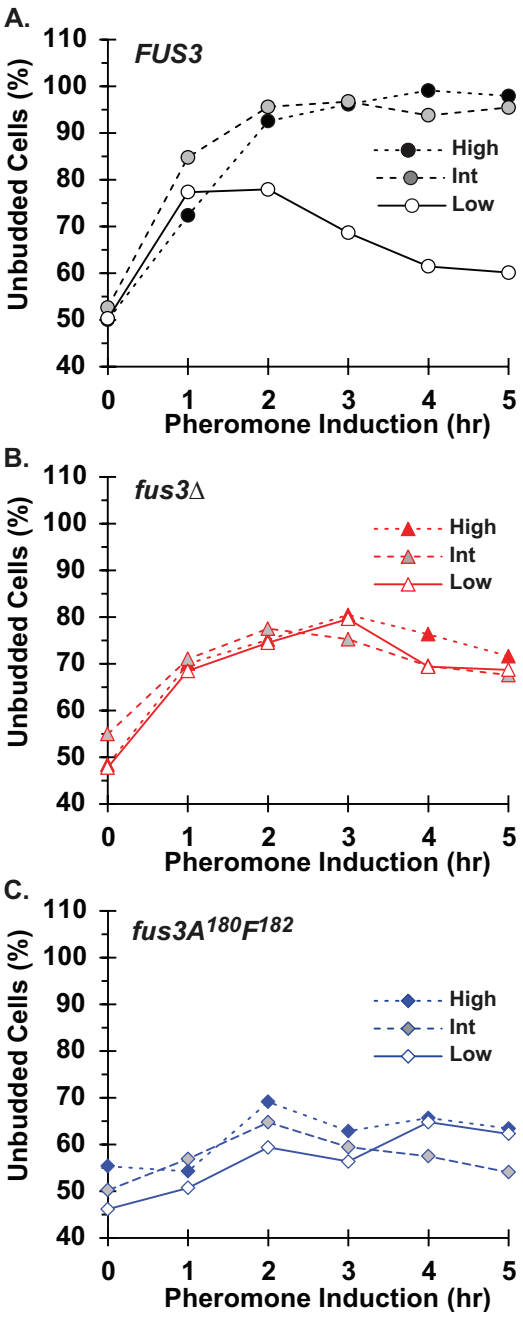

FIGURE 3: G1 arrest efficiency of strains with different *FUS3* alleles in pheromone gradients. The percentage of unbudded cells in the microfluidic chambers used for data shown in Figure 2 was determined at hourly intervals after introduction of the pheromone gradient. (A–C) Unbudded cell percentage vs. time for the upper (black or red symbols; dotted line), intermediate (gray symbols; dashed line), and bottom (white symbols; solid line) one-third of the gradient for the strains with the indicated *FUS3* alleles. The accumulation of unbudded cells is an indication of G1 arrest.

arrest response than do wild-type cells, with only 75–80% accumulating as unbudded cells. Of interest, the arrest response is the same regardless of position in the pheromone gradient (Figure 3B). The arrest response for cells expressing nonactivatable Fus3 (*fus3A^{180}F^{182}*) is also independent of position in the pheromone gradient. However, consistent with a previous study, Fus3A^{180}F^{182}-expressing cells are more refractory to G1 arrest than are cells lacking Fus3 (*fus3*Δ; Figure 3C; Breitkreutz *et al.*, 2001). Thus nonactivatable Fus3 has the capability of more potently inhibiting pheromone-induced mating specific transcription, morphogenesis, and G1 arrest than absence of Fus3 in the cells.

Kss1 dual phosphorylation is elevated in strains without Fus3 activity

The contrasting behavior of cells without Fus3 and those expressing the Fus3 variant support the conclusion that nonactivatable Fus3 is an inhibitor of the mating and chemotropic transitions. One, albeit unlikely, explanation is that some strains compensate for loss of activity from having no or catalytically inert Fus3 by elevating the amount of active Kss1 (Sabbagh *et al.*, 2001; Hao *et al.*, 2012), but this compensation does not occur in the strain background used here. To eliminate this possibility, we compared the dual-phosphorylation status of Fus3 and Kss1 in the strains with different *FUS3* alleles before and at indicated times after pheromone induction. Extracts from samples of the different cultures were fractionated by SDS–PAGE and transferred to nitrocellulose for immune blot analysis to detect the amount of each MAPK that is dually phosphorylated (pT-E-pY) at the activation loop by using anti–phospho-p42/p44 antibodies (Sabbagh *et al.*, 2001). Consistent with previous observations, the *fus3*Δ strain has significantly elevated basal and pheromone-induced amounts of dual-phosphorylated Kss1compared with the *FUS3* reference strain (Figure 4; Sabbagh *et al.*, 2001; Hao *et al.*, 2012). A similar elevation is observed in the *fus3A^{180}F^{182}* strain (Figure 4). This finding is pertinent because it shows that elevated Kss1 activity is insufficient to overcome the inhibitory effect of inactive Fus3 on mating and chemotropic transitions.

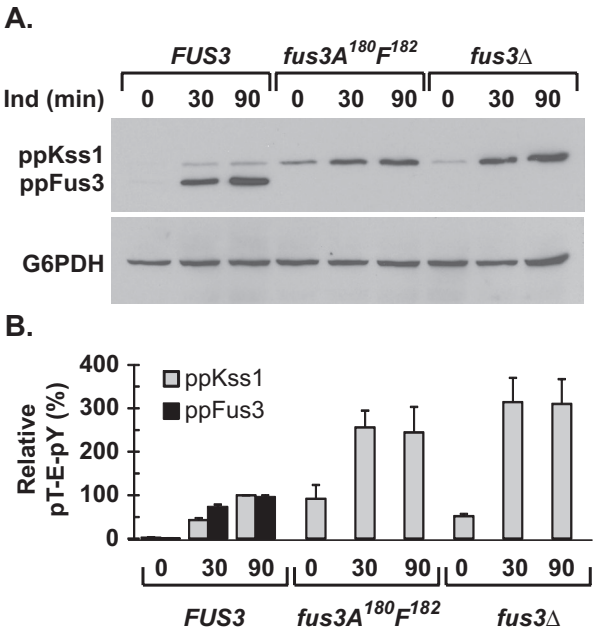

FIGURE 4: Comparison of MAPK dual phosphorylation induced by pheromone in strains with different *FUS3* alleles. (A) Representative immune blots detecting dual-phosphorylated Kss1 and Fus3 by using anti–phospho-p42/p44 (α-pT-E-pY) antibodies (top). G6PDH was used as a loading control and detected by using anti-G6PDH antibodies (bottom). Protein extracts (50 μg) were from cultures of the following strains: *FUS3* (C699-5), *fus3*Δ (C699-200), and *fus3A^{180}F^{182}* (C699-207) before (*t* = 0) and at indicated times after addition of pheromone (50 nM α-fr). (B) Bar graphs comparing the induction of dual-phosphorylated Kss1 (□) and Fus3 (■) in strains with the *FUS3*, *fus3A^{180}F^{182}*, or *fus3*Δ allele as indicated. Values are relative to the time point having maximal signal for the corresponding phospho-MAPK in the strain expressing *FUS3* and are the average of three independent experiments. Error bars show 95% confidence limits.

Activation of the pathway by Ste5-CTM suppresses the morphogenetic but not the transcriptional defect caused by nonactivatable Fus3

Fus3 activity and binding interactions have documented roles in pheromone-induced transcription and morphogenesis (Madhani *et al.*, 1997; Tedford *et al.*, 1997; Bardwell *et al.*, 1998b; Roberts *et al.*, 2000; Metodiev *et al.*, 2002; Matheos *et al.*, 2004; Figure 1). We considered the possibility that the binding of inactive Fus3 to relevant targets could obstruct compensating phosphorylation by Kss1 and therefore result in more severe defects than seen in the complete absence of Fus3. To test whether active receptor and/or G-protein might be the relevant target(s) for the effect that nonactivatable Fus3 has on morphogenesis, we exploited a variant of the scaffold Ste5 that is artificially targeted to the plasma membrane by its fusion to a carboxy-terminal transmembrane (CTM) sequence (Pryciak and Huntress, 1998). Overexpression of this fusion was shown to activate the mating pathway in the absence of pheromone or activated G-protein (Pryciak and Huntress, 1998). We generated isogenic *FUS3*, *fus3*Δ, and *fus3A^{180}F^{182}* strains with Ste5-CTM under control of the galactose-regulated promoter (P_{GAL1}) expressed from the endogenous locus. We then used microfluidic chambers and time-lapse imaging to follow cells during galactose induction of Ste5-CTM.

Cells from the time-lapse images were scored as budded or unbudded (independently of their morphology) to monitor G1 arrest. At the start of the time course (*t* = 0), the raffinose-grown cells for each of the strains in the microfluidic chambers showed a budding index (~35–45% unbudded) typical of mitotic cultures (Figure 5B). Nearly 100% of the reference cells (*FUS3*) were arrested in G1 as unbudded cells after 12 h of galactose induction (Figure 5B). At the same time point, cells lacking Fus3 (*fus3*Δ) showed a less homogeneous G1 arrest response than wild-type cells, with only ~ 65% accumulating as unbudded cells (Figure 5B). Cells expressing nonactivatable Fus3 (*fus3A^{180}F^{182}*) failed to arrest, as they maintained the same unbudded percentage as the mitotic raffinose culture (Figure 5B). Thus the relative robustness of G1 arrest induced by expression of Ste5-CTM in the three strains (*FUS3* > *fus3*Δ > *fus3A^{180}F^{182}*) is the same as seen under pheromone-inducing conditions.

Ste5-CTM expressing cells from the aforementioned images were also scored for cell morphology (vegetative, shmoo, or hyperelongated) as described for the pheromone induction experiments in Figure 2. The population of reference cells (*FUS3*) was heterogeneous with respect to vegetative, elongated, and shmoo morphologies after 12 h of galactose induction (Figure 5C). Cells lacking Fus3 (*fus3*Δ) failed to shmoo but were equally distributed between vegetative and elongated morphologies (Figure 5C). Cells expressing nonactivatable Fus3 (*fus3A^{180}F^{182}*) showed a distribution of vegetative and elongated morphologies that was comparable to that of *fus3*Δ cells (Figure 5C). Thus activation of the pathway by Ste5-CTM

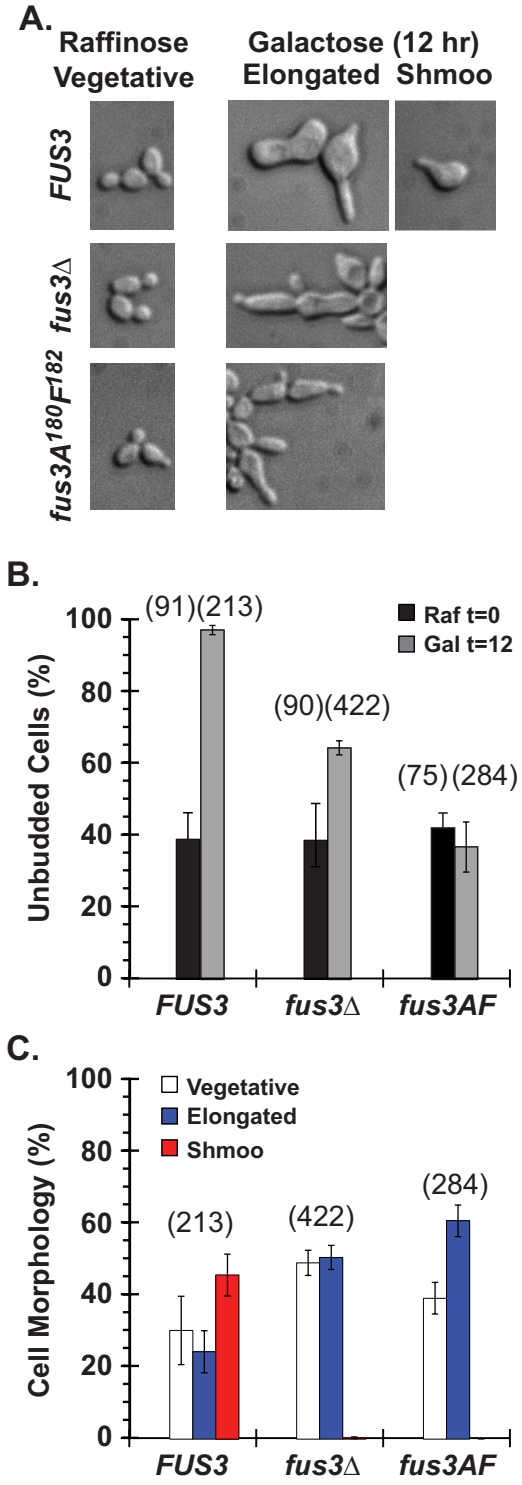

FIGURE 5: Developmental fate morphologies and G1 arrest promoted by overexpression of Ste5-CTM in the absence of pheromone. Cells from *bar1Δ* P_{GAL1}*-STE5-CTM* strains with *FUS3* (C699-218), *fus3Δ* (C699-214), or *fus3A*^{180}*F*^{182} (C699-219) as indicated were grown in raffinose medium and switched to uniform 2% galactose medium in microfluidic chambers to induce overexpression of Ste5-CTM. (A) Micrographs of cells in the chambers before (t = 0) and after switching to 2% galactose medium (t = 12 h) show representative morphologies of the indicated categories used for scoring. (B) Bar graph comparing unbudded cell percentage (independent of morphology) in raffinose at the start of the time course (■) and 12 h after switching to 2% galactose (▨). Total number of cells scored at t = 0 and 12 h is given above the bars. (C) Bar graph comparing percentage of cells in galactose (t = 12 h) that have vegetative (□), hyperelongated (■), or shmoo (■) morphology (independent of budding status). Total number of cells scored is given above the bars for each *FUS3* allele. Error bars in B and C show 95% confidence limit using data from three experiments.

masks the inhibitory effect of nonactivatable Fus3 on morphogenesis. This outcome points to a role for Fus3 in morphogenesis at the level of the active receptor or G-protein.

We also compared expression of the prototypical mating-specific reporter gene (*PRE$_3$-lacZ*) in these three strains after 8 h of growth in galactose medium (Table 1). In contrast to reporter expression induced by pheromone, *PRE$_3$-lacZ* expression activated by Ste5-CTM was significantly less in cells without Fus3 (*fus3Δ*) than in the reference cells (*FUS3*; Table 1). We infer that Kss1 may be less potently activated by targeting Ste5 to the membrane than by pheromone induction. Nevertheless, the strain expressing nonactivatable Fus3 (*fus3A*^{180}*F*^{182}) has much lower reporter gene expression (nearly baseline) than even the strain without Fus3 (*fus3Δ*) (Table 1). Thus, in Ste5-CTM–expressing strains, nonactivatable Fus3 inhibits transcription but not the morphological transition. This outcome reveals that Fus3 regulates morphogenesis and transcription by independent mechanisms.

The binding of nonactivatable Fus3 to Gα inhibits pheromone-induced morphogenesis

It was previously shown that Fus3 binds directly to the Gα subunit of the activated G-protein (Metodiev *et al.*, 2002). This interaction poises Fus3 for phosphorylating the formin homologue Bni1, which in turn promotes actin assembly and polarized growth (Matheos *et al.*, 2004; Figure 1). To test whether binding to Gα underlies the effect that nonactivatable Fus3 has on morphogenesis, we exploited a MAPK-docking-site Gα variant (Gpa1E^{21}E^{22}) that abrogates binding (Metodiev *et al.*, 2002) and generated isogenic *FUS3*, *fus3Δ*, and *fus3A*^{180}*F*^{182} strains with the *GPA1E*^{21}*E*^{22} allele expressed from the endogenous locus. As before, we used microfluidic chambers to expose cells to a pheromone gradient (5–50 nM) over a 5-h time course. After 5 h in the pheromone gradient, the strain coexpressing the nonactivatable Fus3 and Gα nondocking variants (*fus3A*^{180}*F*^{182} *GPA1E*^{21}*E*^{22}) showed the same distribution of elongated and vegetative cells as did the strains devoid of Fus3 either with or without the Gα nondocking variant (*fus3Δ GPA1E*^{21}*E*^{22}, *fus3Δ GPA1*; Figures 6, B and C, and 2B). We conclude that binding of nonactivatable Fus3 to Gpa1 leads to its negative effect on morphogenesis. This effect is not observed in the absence of Fus3 because Kss1 has free access to the critical targets and is able to compensate.

Fus3 binding to Gα is required for gradient tracking and suppression of noise in the morphogenetic response to pheromone

The reference strain expressing the Gα nondocking variant (*FUS3 GPA1E*^{21}*E*^{22}) exhibited different pheromone gradient behavior from that of the wild-type strain (*FUS3 GPA1*; compare Figures 6A and 2B). One striking difference for the *FUS3 GPA1E*^{21}*E*^{22} strain was the apparent inability of cells to track a gradient. To assess gradient tracking quantitatively, we focused on cells residing in the intermediate zone of chamber, where the pheromone gradient is most linear. Cell polarization was quantified by measuring the final angle of polarized growth and is represented as an angle distribution

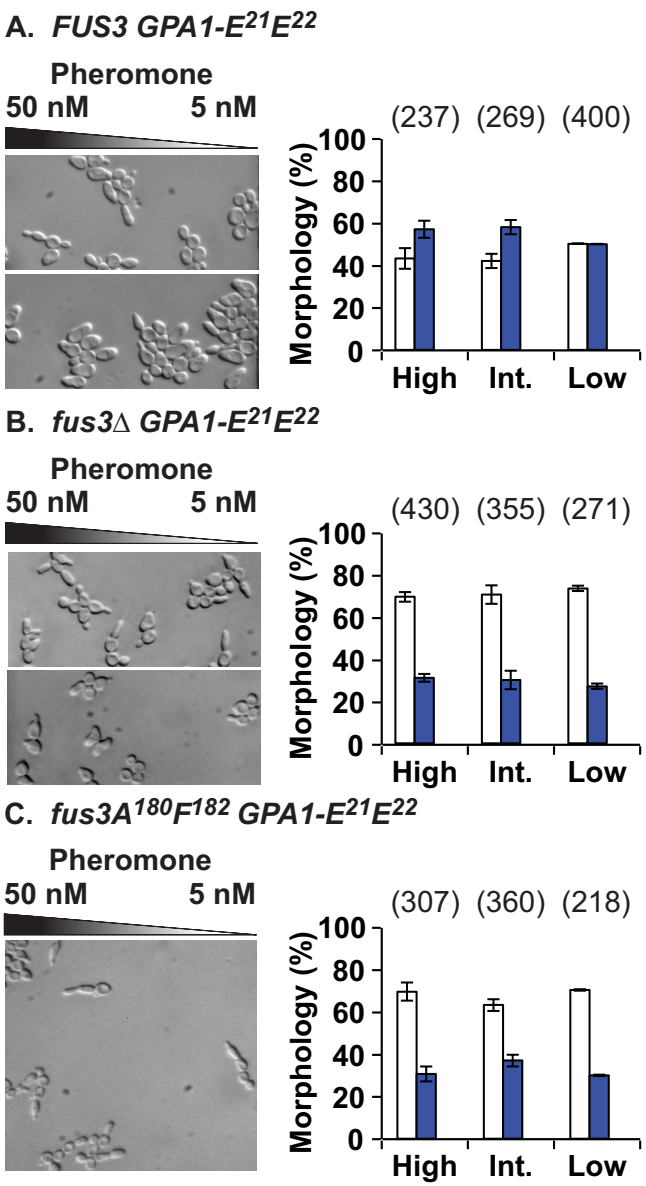

FIGURE 6: Developmental fate morphologies of *GPA1-E*^{21}*E*^{22} strains with different *FUS3* alleles in pheromone gradients. Cells from *bar1*Δ *GPA1-E*^{21}*E*^{22} strains with *FUS3* (C699-223), *fus3*Δ (C699-331), or *fus3A*^{180}*F*^{182} (C699-221) as indicated were exposed to a linear gradient of pheromone (50–5 nM) in microfluidic chambers. (A–C) Left, micrographs showing representative fields of cells with the indicated *FUS3* alleles after 5 h of growth in pheromone gradient chambers. Right, bar graphs showing the percentage of cells in the upper (High), intermediate (Int), or lower (Low) one-third of the gradient with vegetative (□) or hyperelongated (■) morphology after 5 h of exposure to pheromone. (A) <1% of the cells at High and Int. pheromone were scored as shmoos; (B and C) no cells scored as shmoos. Error bars show the 95% confidence limit for data from three or more gradient chamber experiments. The total number of cells scored in each portion of the gradient is given above the bars. Micrographs of cells in Figure 2D illustrate representative morphologies of the indicated categories used for scoring.

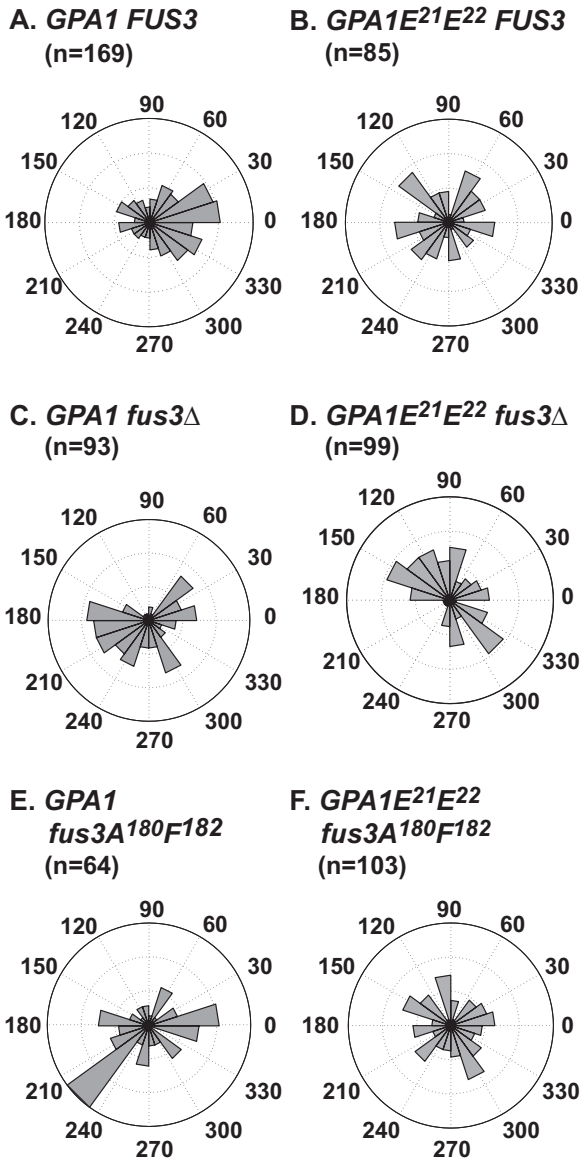

FIGURE 7: Comparison of gradient tracking in *GPA1* and *GPA1E*^{21}*E*^{22} strains with different *FUS3* alleles. Histograms show the frequency distribution of the angle of cell polarization with respect to the pheromone gradient for the strains analyzed in Figures 2 and 6 after 4.5 h of growth in the gradient chambers. Zero degrees represents perfect alignment toward the gradient. Histograms report the percentage of cells with the angles (in degrees) as specified for each wedge on the circle periphery. The scale for cell percentage (0–15%) is indicated by rings emanating from the center of the circle. Data were collected from three or more independent experiments. Only cells in the intermediate zone of the gradient chamber were scored; the number scored (*n*) for each strain is given above the corresponding histogram.

histogram (Figure 7). As expected, wild-type cells (*FUS3 GPA1*) oriented their growth in the direction of high pheromone, typically within ±45° of the gradient (Figure 7A). By contrast, cells expressing the Gα nondocking variant (*FUS3 GPA1E*^{21}*E*^{22}) oriented randomly (Figure 7B). The random growth orientation of the *FUS3 GPA1E*^{21}*E*^{22} cells in the gradient is typical of cells without Fus3 activity (Hao *et al.*, 2008; Figure 7, C–F. Taken together, these results show that the docking of Fus3 on Gα is essential for chemotropism.

Another difference for the strain expressing the Gα nondocking variant was the absence of a significant number of shmoos even in the high-concentration region of the gradient. Such a defect could be attributed to decreased sensitivity to pheromone. To assess this

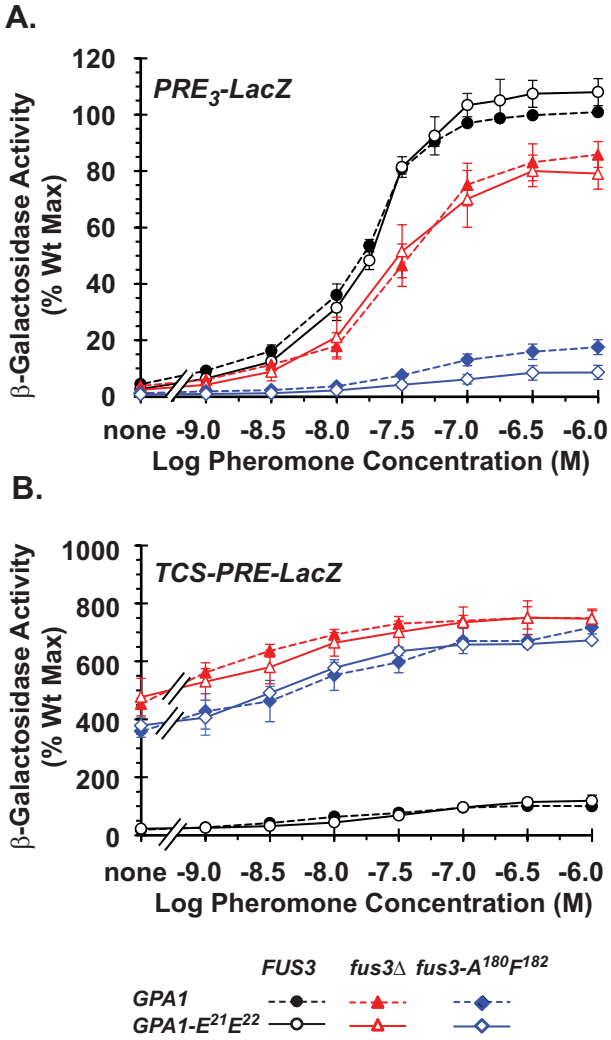

FIGURE 8: Comparison of transcription dose responses in *GPA1* and *GPA1E*^{21}*E*^{22} strains with different *FUS3* alleles. (A, B) Plots of indicated reporter gene expression vs. pheromone dosage, (0–1) × 10^{-6} M α-factor. β-Galactosidase activity was measured using cultures of *bar1*Δ strains *FUS3 GPA1* (C699-5), *fus3*Δ *GPA1* (C699-200), *fus3A*^{180}*F*^{182} *GPA1* (C699-207), *FUS3 GPA1-E*^{21}*E*^{22} (C699-223), *fus3*Δ *GPA1-E*^{21}*E*^{22} (C699-331), and *fus3A*^{180}*F*^{182} *GPA1-E*^{21}*E*^{22} (C699-221) carrying the *PRE*$_3$*-LacZ* (pGA1706) or *TCS-PRE-LacZ* (pNC343) reporter gene plasmid after 90 min of induction with indicated concentrations of pheromone. Data points are the mean of four (A) or three (B) independent experiments. Error bars show the 95% confidence limit. *FUS3*, circles; *fus3*Δ, triangles; *fus3A*^{180}*F*^{182}, diamonds; *GPA1* strains, solid symbols with dashed lines; *GPA1E*^{21}*E*^{22} strains, open symbols with solid lines.

possibility, we conducted dose-response comparisons for transcription using the reporter gene representative of the mating program (*PRE*$_3$*-LacZ*). Reporter expression was measured after 90 min of incubation of cells with pheromone at concentrations ranging from 1.0 × 10^{-6} to 1.0 × 10^{-9} M (log scale –6.0 to –9.0). Reference samples without added pheromone were included in the analysis. The profiles show the expected trends for strains with wild-type Fus3 (*FUS3*), no Fus3 (*fus3*Δ), or nonactivatable Fus3 (*fus3A*^{180}*F*^{182}). Of importance, profiles are essentially the same whether strains express wild-type Gα(*GPA1*) or the nondocking variant (*GPA1E*^{21}*E*^{22}; Figure 8A). For comparison, the analysis was done using the reporter gene representative of the filamentation program (*TCS-PRE-LacZ*). Typical of Kss1-promoted responses, the amount of reporter expression is relatively insensitive to pheromone dosage. Again the profiles show the expected trends for the different *FUS3* alleles and are essentially the same whether strains express wild-type Gα(*GPA1*) or the nondocking variant (*GPA1E*^{21}*E*^{22}; Figure 8B).

Results with Ste5-CTM given earlier revealed that transcription and morphogenesis can be regulated independently. Therefore we also assessed dose-response behavior of the *GPA1* and *GPA1E*^{21}*E*^{22} strains with different *FUS3* alleles for G1 arrest and morphogenesis. For these experiments, parallel cultures were treated with pheromone at concentrations ranging from 3.2 × 10^{-7} to 3.2 × 10^{-9} M (log scale –6.5 to –8.5). After 5 h, cells were fixed in formaldehyde and scored for cells in G1 (unbudded cells, independently of morphology) and polarized growth characteristic of pheromone response (either hyperelongated or shmoo, independently of budding). These comparisons show that there is no difference in the dosage dependence for the G1-arrest response based on whether the strains with different *FUS3* alleles express wild-type Gα (*GPA1*) or the nondocking variant (*GPA1E*^{21}*E*^{22}; Figure 9A). There was no difference in the percentage of *FUS3* or *fus3*Δ cells exhibiting polarized growth, which depended on whether cells had the *GPA1* or *GPA1E*^{21}*E*^{22} allele (Figure 9B). However, the percentage of *fus3A*^{180}*F*^{182}*GPA1* cells exhibiting polarized growth was significantly less at all pheromone concentrations than for the *fus3A*^{180}*F*^{182}*GPA1E*^{21}*E*^{22} cells. Of importance, the pheromone dependence of polarized growth for the strain coexpressing the nonactivatable Fus3 and nondocking Gα variants (*fus3A*^{180}*F*^{182}*GPA1E*^{21}*E*^{22}) was indistinguishable from that of the strains without Fus3 (*fus3*Δ; Figure 9B).

We did not distinguish between shmoo and hyperelongated morphologies for the purpose of assessing dose response of the different strains for polarized growth. However, we did observe a significant difference between the *GPA1 FUS3* and *GPA1E*^{21}*E*^{22}*FUS3* strains upon assessing the fraction of responding cells that have a shmoo compared with a hyperelongated morphology (Figure 9C). Specifically, the dose for transition of the population from hyperelongated to shmoo morphology is sharper for *GPA1* cells than for *GPA1E*^{21}*E*^{22}. As a consequence, there is a more heterogeneous distribution of morphologies over a broader range of pheromone concentrations for the cells expressing the nondocking Gα variant compared with wild type. This behavior shows that the binding of Fus3 to Gα reduces heterogeneity and has a noise-suppressing effect on morphogenesis.

DISCUSSION

A Fus3–Gα complex regulates gradient tracking and morphogenesis

To further define regulatory roles for pheromone-activated MAPKs in chemotropism, we compared the pheromone-induced responses of transcription, G1 arrest, and morphogenesis under conditions in which Kss1 is active either in the absence of Fus3 (*fus3*Δ) or the presence of a Fus3 variant that is inactive because it cannot be phosphorylated (*fus3A*^{180}*F*^{182}; Gartner *et al.*, 1992). These comparisons revealed a previously unappreciated role for inactive Fus3 as a negative regulator of pheromone-induced chemotropism. The analyses further showed that Fus3 binding to the G-protein α-subunit is required for gradient tracking and acts to suppress cell-to-cell variability between mating and chemotropic fates in a population of pheromone-responding cells.

To explain these observations, we speculate that Gα provides a docking motif that serves to colocalize Fus3 with a substrate whose phosphorylation is critical for morphogenesis. We assume that the

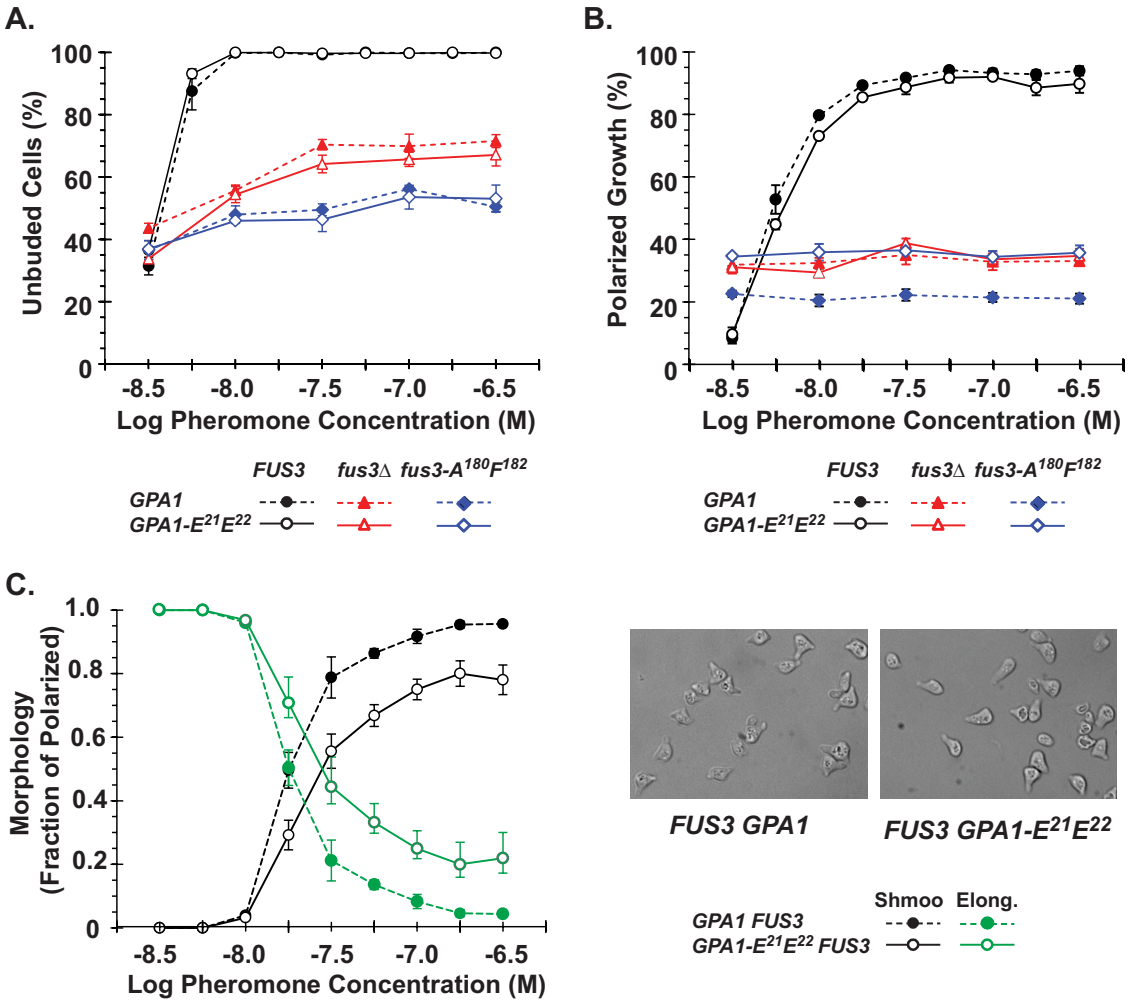

FIGURE 9: Comparison of G1 arrest and morphological dose responses in *GPA1* and *GPA1E*^{21}*E*^{22} strains with different *FUS3* alleles. Budding and cell morphologies were scored for strains (as specified in the legend to Figure 8) with the indicated alleles using formaldehyde-fixed aliquots of cultures after 5 h of incubation at indicated concentrations of pheromone (3×10^{-9} to 3×10^{-7} M α-factor). (A) Plots of the percentage of G1 (unbudded) cells vs. log pheromone concentration. (B) Plots of the percentage of cells with pheromone-induced polarized growth (either hyperelongated or shmoo) vs. log pheromone concentration. (C) Left, plots comparing the fraction of responding cells with hyperelongated (green lines and symbols) or shmoo morphology (black lines and symbols) vs. log pheromone concentration. Right, micrographs showing a representative field of *GPA1* and *GPA1E*^{21}*E*^{22} cells as indicated. Error bars show 95% confidence limit. *FUS3*, circles; *fus3*Δ, triangles; *fus3A*^{180}*F*^{182}, diamonds; *GPA1* strains, solid symbols with dashed lines; *GPA1E*^{21}*E*^{22} strains, open symbols with solid lines.

MAPK docking site on Gα binds to Fus3 but poorly or not at all to Kss1. We further speculate that the target to be phosphorylated lacks a MAPK docking motif. This colocalization of the three components increases the efficiency of target phosphorylation (Figure 10A, top). In the case in which Fus3 is absent, a ternary complex does not form, so that Kss1 has access to the target. In this case, the phosphorylation reaction may not be as efficient as when colocalization is imposed by docking to Gα (Figure 10A, middle). A stable complex between inactive Fus3 and Gα would impose steric constraints for access of other kinases to that target. As such, the inactive ternary complex physically obstructs Kss1 from phosphorylating the target substrate. In the unphosphorylated state, the target is unable to promote morphogenesis (Figure 10A, bottom).

In the case in which there is active Fus3 but it is prevented from docking on Gα (by mutation of the docking site), both Fus3 and Kss1 have access to the target. However, without the ternary complex, the phosphorylation reaction may not be as efficient as when colocalization is imposed (Figure 10B, top). The reduced efficiency in target protein phosphorylation by Fus3 or the more significant competition with Kss1 could underlie a greater heterogeneity in shmoo versus hyperelongated morphology compared with when Gα has a functional docking site for Fus3. The morphogenesis phenotype of a strain expressing nonactivatable Fus3 reverts to that of the strain devoid of Fus3 simply by masking the Gα MAPK docking site. This masking can occur either by bypassing G-protein activation, as seen with Ste5-CTM, or by introducing amino acid substitutions in the Gα MAPK docking site that eliminate the Fus3–Gα binding interaction. In either case, the phenotype is reversed specifically because there is no ternary complex to obstruct Kss1 from phosphorylating the target (Figure 10B, middle and top.) An obvious candidate for a critical substrate is Bni1 because its phosphorylation by Fus3 has a known role in pheromone-induced morphogenesis

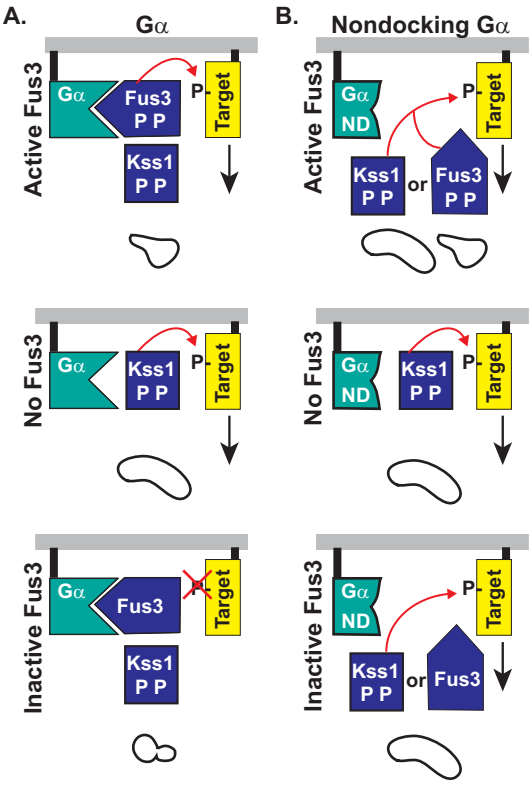

FIGURE 10: Schematic representation of a ternary complex postulated to facilitate target protein phosphorylation (P-Target) that is required for pheromone induced morphogenesis. (A) Interactions in the context of wild-type Gα. (B) Interactions in the context of a nondocking Gα variant (GαND). Scenarios with dual-phosphorylated and catalytically active Fus3 (Fus3PP; top), no Fus3 (middle), and inactive Fus3 that cannot be phosphorylated (Fus3; bottom). Dual-phosphorylated Kss1 (Kss1PP) is an active kinase that does bind to the Gα docking motif. See the text for an explanation.

(Matheos *et al.*, 2004). Other targets may be septins or septin-associated proteins because of their role in gradient tracking (Kelley *et al.*, 2015).

The Gα nondocking variant does not suppress the inhibitory effect of inactive Fus3 on mating-specific reporter expression. If the inhibition by inactive Fus3 at the transcriptional level also occurs through a docking interaction, it involves a different binding partner(s). Potentially, the targets could be the Dig1 or Dig2 repressors of Ste12 transcription, both of which are known Fus3 binding partners and substrates (Tedford *et al.*, 1997). However, other mechanisms for transcriptional inhibition by inactive Fus3 that do not involve steric hindrance effects on Kss1 remain possible.

Two additional insights emerged from our efforts to understand how inactive Fus3 inhibits the chemotropic response. First, the binding of Fus3 to Gα is required for cells to track a pheromone gradient. This conclusion was drawn from live-cell imaging of a strain expressing wild-type Fus3 and a nondocking Gα variant in a pheromone gradient. These results validate the deduction based on mating partner discrimination assays that were used before the availability of the current technology (Metodiev *et al.*, 2002). An implication of this requirement for gradient tracking is that the interaction with Gα poises Fus3 for phosphorylation of target proteins involved in regulating polar cap mobility and septin deposition (Kelley *et al.*, 2015). Second, the binding of Fus3 to Gα serves to suppress cell-to-cell variability in pheromone-induced morphogenesis. Normally, the pheromone dose at which cells transition from chemotropic to shmoo morphology is relatively sharp. Consequently the population distribution at a given pheromone concentration is fairly homogeneous for one type or the other. However, disruption of the Fus3–Gα binding interaction results in a more heterogeneous distribution of the two morphologies over a broader range of pheromone concentrations.

The importance of a MAPK–Gα docking interaction in developmental decisions is not unique to the yeast mating pathway. The soil amoeba *Dictyostelium discoideum* has 12 different Gα subunits and two MAPKs. Recently, roles for Erk1 or Erk2 binding to two of the Gα subunits have been found to be important during multicellular development of this organism. Gα4 binding to Erk2 was shown to be required for morphogenesis associated with culmination but not for its chemotaxis to folate (Nguyen and Hadwiger, 2009). Gα5 binding to Erk1 was similarly found to be important for Gα5 function in regulation of aggregate formation and tip development but not in the inhibition of folate chemotaxis (Raisley *et al.*, 2010). Raisley *et al.* (2010) identified the presence of MAPK-docking sites in Gα subunits of not only yeast and *Dictyostelium*, but also mammalian cells. They highlighted the implication that MAPK interactions with Gα subunits might be widespread among eukaryotes and are likely to play important roles in G-protein–coupled receptor signaling.

Specialized functions for MAPK isoforms

It has been appreciated for some time that Fus3 and Kss1 have specialized regulatory roles in the mating differentiation and invasive growth transitions. The positive regulatory role of active Fus3 in the establishment of a stable G1 arrest and formation of mating projections explains why strains lacking Fus3 (*fus3*Δ) only transiently arrest in G1 and are unable to produce mating projections in response to saturating pheromone (Elion *et al.*, 1990, 1991). Both Fus3 and Kss1 positively regulate Ste12 transcriptional activity at pheromone-inducible genes by phosphorylating and destabilizing the repressor complex formed with Dig1 and Dig2 at these promoters (Madhani *et al.*, 1997; Tedford *et al.*, 1997; Bardwell *et al.*, 1998b; Roberts *et al.*, 2000). Active Fus3 also specifies Ste12 promoter selectivity under pheromone-induced conditions through phosphorylation of Tec1 and its subsequent SCF-catalyzed ubiquitination and degradation (Bao *et al.*, 2004; Bruckner *et al.*, 2004; Chou *et al.*, 2004; Wang and Dohlman, 2006). This additional regulatory role for active Fus3 promotes the transcriptional program specifying mating differentiation while inhibiting the program specifying invasive growth. Impairment of Tec1 turnover also accounts for the hyperinvasive growth phenotype of *fus3*Δ strains (Cook *et al.*, 1997). Kss1 has both negative and positive regulatory roles in the invasive growth transition. Inactive Kss1 binds directly to Ste12 and stabilizes the Dig1-Ste12-Tec1 repressor complex at filamentation-specific genes (Madhani *et al.*, 1997; Tedford *et al.*, 1997; Bardwell *et al.*, 1998a). Ste7 phosphorylation of Kss1 both promotes Kss1 catalytic activity and weakens Kss1–Ste12 binding. Kss1 phosphorylation of Dig1 (and Dig2) is believed to have a positive role in regulating transcription of filamentation-specific genes analogous to its role in regulating transcription of mating-specific genes (Cook *et al.*, 1996; Tedford *et al.*, 1997).

The roles of Fus3 and Kss1 in the chemotropic transition are less well studied. Strains lacking Fus3 (*fus3*Δ) respond to (high and low) pheromone by transiently arresting in G1 and adopting an elongated morphology even though they are unable to track pheromone gradients. The elongated morphology of *fus3*Δ strains is attributed to an overlapping function provided by Kss1, which becomes hyperactivated in the absence of Fus3 activity. In contrast to

fus3Δ strains, strains expressing nonactivatable Fus3 (Fus3-$A^{180}F^{182}$) proliferate and retain largely vegetative morphology in the presence of pheromone. The contrasting phenotype of strains with nonactivatable Fus3 compared with strains lacking Fus3 reveals an inhibitory role for the inactive kinase in the pheromone-induced chemotropic program.

Chemotropism in low pheromone gradients is believed to increase the probability of an encounter with a distant mating partner (Erdman and Snyder, 2001). The extensive growth entailed in this search undoubtedly requires significant energy expenditure. Because Kss1 supports elongated growth but not gradient tracking (Hao *et al.*, 2008), the inhibition by inactive Fus3 provides a beneficial "checkpoint" to guard against futile elongation and adds a layer of insulation between the invasive growth and mating pathways.

Unraveling the regulatory roles for the MAPKs Fus3 and Kss1 in different fate transitions will reveal aspects of signaling circuitries that are likely to be more broadly relevant to MAPK-mediated mammalian development. Erk1 and Erk2 are generally believed to possess redundant or overlapping functions because they are coactivated in mammalian cells in response to multiple stimuli. However, several reports revealed scenarios in which there are specialized roles for the different isoforms. For example, Erk1 appears to have a more important role in osteoclast development and bone resorptive activity (He *et al.*, 2011) and thymocyte maturation (Fischer *et al.*, 2005), whereas Erk2 has essential roles in mesoderm development, including myogenesis (Sarbassov *et al.*, 1997) and the epithelial to mesenchymal transformation (Shin *et al.*, 2010). Recent studies using genetic ablation of Erk1 or Erk2 revealed differences in T-cell proliferation, expansion, and differentiation, depending on which Erk is inactivated (Chang *et al.*, 2012). Studies on the mechanisms through which Erk1 and Erk2 regulate transcription in pancreatic β-cells revealed that the kinases themselves are components of chromatin-bound transcription factor complexes on both the insulin and c-fos genes. In this example, the kinases appear on promoters when they are active and are no longer captured on chromatin if their activity is blocked (Lawrence *et al.*, 2008). Evidence is also accumulating that Erk1 and Erk2 can play functionally important roles in chromatin remodeling, DNA transcription, and cell cycle regulation independently of their regular catalytic activities (for review, see Rodriguez and Crespo, 2011). The finding of context-specific MAPK functions in mammals indicates that the mechanisms underlying those for fate decisions in yeast are likely conserved.

MATERIALS AND METHODS

Plasmids

The plasmids used in these studies have been described previously. Table 2 provides their source and/or reference.

Yeast strains and genetic procedures

Table 3 lists yeast strains used in these studies. Table 4 lists the sequence of oligonucleotides used for PCR fragment amplification, mutagenesis, and DNA sequence confirmation involved in the construction of these strains. Media preparation and standard yeast genetic methods for transformation, gene replacement, crosses, and tetrad dissection were as described in Amberg *et al.* (2005).

The following two strains were constructed using the one-step gene replacement method (Rothstein, 1983). C700-5 was derived from C700 by using the *Eco*RI–*Sal*I fragment from pJGsst1 (Reneke *et al.*, 1988) to replace the *BAR1* locus with the *bar1Δ::hisG-URA3-hisG* allele. The *bar1Δ::HisG* allele was generated from the resulting strain by selection on 5-fluoroorotic acid (Life Technologies, Grand Island, NY) medium (Boeke *et al.*, 1994). This medium provides a positive selection for isolates in which the *URA3* marker is excised by recombination within the direct *hisG* repeats (Alani *et al.*, 1987). Strain C699-200 was derived from C699-5 by replacing the *FUS3* locus with the *fus3Δ6::LEU2 Hin*dIII fragment from pYEE98 (Elion *et al.*, 1990).

Strain C699-188 is a segregant resulting from a cross between strains C699-106 (Maleri *et al.*, 2004) and C700-5. To make this cross, C699-106 was transformed with pNC752 (*STE7*) (Maleri *et al.*, 2004) to complement the *ste7Δ::hisG* mutation. This complementation allowed selection of zygotes from mating mixtures with strain C700-5. Diploid isolates that lost the plasmid after nonselective growth were used for tetrad dissection and analysis of segregants from the cross. The presence of the *STE7* allele in C699-188 was confirmed using yeast colony PCR analysis with oligonucleotide primers 350 and 1031 (Akada *et al.*, 2000).

Plasmid	Allele	Vector	Source or reference
pCORE-UK	*^{KI}URA3::KanMX4*		Storici and Resnick (2006)
pCR Blunt II Topo			Invitrogen Life Technologies
pGA1706	*PRE_3-lacZ*	pLGΔ178	Baur *et al.* (1997)
pGA1895	*fus3T^{180}A,Y^{182}F*	pNC160	Gartner *et al.* (1992)
pJGsst1	*bar1::hisG-URA3-hisG*		Reneke *et al.* (1988)
pLGΔ178	*(CYC1ΔUAS)-lacZ*		Guarente *et al.* (1984)
pNC160	*TRP1-ARS1 CEN3*		Rhodes *et al.* (1990)
pNC343	*TCS-PRE–lacZ*	pLGΔ178	Baur *et al.* (1997)
pNC752	*STE7M*	pNC160	Maleri *et al.* (2004)
pGS5-CTM	*P_{GAL1}-STE5CTM*	pRS314	Pryciak and Huntress (1998)
pRS313	*HIS3 CEN6 ARSH4*		Sikorski and Hieter (1989)
pRS314	*TRP1 CEN6 ARSH4*		Sikorski and Hieter (1989)
pYEE81	*FUS3*	YCp50	Elion *et al.* (1990)
pYEE98	*fus3Δ6::LEU2*		Elion *et al.* (1990)
YCp50	*URA3 ARS1 CEN4*		Johnston and Davis (1984)

TABLE 2: Plasmids.

Strain[a]	Genotype	Source or reference
C699	*MAT***a** *ade2-1 can1-100 his3-11,15 leu2-3112 trp1-1 ura3-1*	K. Nasmyth, University of Oxford, UK
C699-5	*MAT***a** *ade2-1 can1-100 his3-11,15 leu2-3112 trp1-1 ura3-1 bar1Δ::hisG*	Esch and Errede (2002)
C600-106	*MAT***a** *ade2-1 can1-100 his3-11,15 leu2-3112 trp1Δ::HIS3MX6 ura3-1 bar1Δ::hisG ste7Δ4::hisG*	Maleri *et al.* (2004)
C699-188	*MAT***a** *ade2-1 can1-100 his3-11,15 leu2-3112 trp1Δ::HIS3MX6 ura3-1 bar1Δ::hisG*	This work
C699-192	*MAT***a** *ade2-1 can1-100 his3-11,15 leu2-3112 trp1Δ::HIS3MX6 ura3-1 bar1Δ::hisG fus3T^{180}A,Y^{182}F*	This work
C699-200	*MAT***a** *ade2-1 can1-100 his3-11,15 leu2-3112 trp1-1 ura3-1 bar1Δ::hisG fus3Δ6::LEU2*	This work
C699-207	*MAT***a** *ade2-1 can1-100 his3-11,15 leu2-3112 trp1-1 ura3-1 bar1Δ::HisG fus3T^{180}A,Y^{182}F*	This work
C699-214	*MAT***a** *ade2-1 can1-100 his3-11,15 leu2-3112 trp1-1 ura3-1 bar1Δ::hisG fus3Δ6::LEU2 P$_{GAL1}$-STE5-CTM*	This work
C699-218	*MAT***a** *ade2-1 can1-100 his3-11,15 leu2-3112 trp1-1 ura3-1 bar1Δ::hisG FUS3 P$_{GAL1}$-STE5-CTM*	This work
C699-219	*MAT***a** *ade2-1 can1-100 his3-11,15 leu2-3112 trp1Δ::HIS3MX6 ura3-1 bar1Δ::hisG fus3T^{180}A,Y^{182}F P$_{GAL1}$-STE5-CTM*	This work
C699-221	*MAT***a** *ade2-1 can1-100 his3-11,15 leu2-3112 trp1-1 ura3-1 bar1Δ::hisG fus3T^{180}A,Y^{182}F GPA1E^{21},E^{22}*	This work
C699-223	*MAT***a** *ade2-1 can1-100 his3-11,15 leu2-3112 trp1-1 ura3-1 bar1Δ::hisG FUS3 GPA1E^{21},E^{22}*	This work
C699-331	*MAT***a** *ade2-1 can1-100 his3-11,15 leu2-3112 trp1-1 ura3-1 bar1Δ::hisG fus3Δ6::LEU2 GPA1E^{21},E^{22}*	This work
C700	*MATα ade2-1 can1-100 his3-11,15 leu2-3112 trp1-1 ura3-1*	K. Nasmyth
C700-5	*MATα ade2-1 can1-100 his3-11,15 leu2-3112 trp1-1 ura3-1 bar1Δ::hisG*	This work
C700-29	*MATα ade2-1 can1-100 his3-11,15 leu2-3112 trp1-1 ura3-1 bar1Δ::hisG GPA1E^{21},E^{22}*	This work

[a]C699-x and C700-x strains are isogenic to W303-1A.

TABLE 3: *S. cerevisiae* strains.

The following *fus3A^{180}F^{182}*, *P$_{Gal1}$STE5-CTM*, and *GPA1E^{21}E^{22}* strains were constructed in two steps using the "delitto perfetto" approach for in vivo site-directed mutagenesis as described by Storici and Resnick (2006). The first step for construction of *fus3A^{180}F^{182}* strains C699-192 and C699-207 was to replace the *FUS3* locus of strains C699-188 and C699-5, respectively, with a *fus3Δ$^{180\text{-}185}$::CORE-UK* allele. pCORE-UK (Storici and Resnick, 2006) was the template for the first round of PCR synthesis with primers 913 and 914. The resulting PCR product served as template for the second round with primers 925 and 926. Colony PCR analysis using yeast genomic DNA as template with primers 629 and 881 confirmed replacement of *FUS3* codons 180–185 with the *ste5Δ$_0$::CORE-UK* allele in the resulting strains (Akada *et al.*, 2000). In the second step, the *Nde*I–*Bam*HI fragment from pGA1895 (Gartner *et al.*, 1992) replaced the *fus3Δ$^{180\text{-}185}$::CORE-UK* allele with the *fus3A^{180}F^{182}* allele. The gene replacement in C699-192 and C699-207 was confirmed by amplifying the *fus3A^{180}F^{182}* coding region using genomic DNA as the template with primers 937 and 938. The resulting PCR products were sequenced using primer 939.

The first step in the construction of *GPA1E^{21}E^{22}* strain C699-221 involved transformation of strain C699-207 with a *gpaΔ$^{21\text{-}22}$::CORE-UK* allele that was generated in two rounds of PCR. The first round used pCORE-UK (Storici and Resnick, 2006) as DNA as template with primer pair 1216 and 1217. The resulting PCR product served as template for the second round with primers 1218 and 1219. Colony PCR using primers 1223 and 1148 confirmed the integration of *gpaΔ$^{21\text{-}22}$::CORE-UK* at the *GPA1* locus (Akada *et al.*, 2000). In the second step, the *gpa1Δ$^{21\text{-}22}$::CORE-UK* allele was replaced with a 140–base pair fragment extending from 34 base pairs 5′ to the *GPA1* ATG codon through codon 35 by transformation. This allele contains a silent mutation at codon 14 that introduces a *Bam*HI site and codons for glutamate at positions 21 (GAA) and 22 (GAG). The allele was generated by annealing oligonucleotides 1220 and 1221 and extending them with primers 1222 and 1219. Colony PCR using primers 1223 and 1224 to amplify 1036 base pairs of the *GPA1* locus followed by *Bam*HI digestion was used to confirm replacement of the *gpa1Δ$^{21\text{-}22}$::CORE-UK* in strain C699-221. The 1036–base pair amplified fragment from *GPA1E^{21}E^{22}* confirmed isolates was cloned into the pCR Blunt II Topo vector (Invitrogen Life Technologies, Grand Island, NY) and sequenced using M13R and M13F primers to confirm the codon replacements and the fidelity of the locus encompassing the region of mutagenesis.

Strains C700-29 and C699-223 are *MATα FUS3 GPA1E^{21}E^{22}* and *MAT***a** *FUS3 GPA1E^{21}E^{22}* segregants, respectively, from a cross between strains C699-221 (*MAT***a** *fus3A^{180}F^{182} GPA1E^{21}E^{22}*) and C700-5 (*MATα FUS3GPA1*). To make this cross, C699-221 was transformed with YpEE81 [*FUS3 URA3*] to complement the nonmating phenotype of the *fus3A^{180}F^{182}* mutant strain. and C700-5 was transformed with pRS313 [*HIS3*] to allow nutritional selection of diploids from mating mixtures on synthetic medium (SD) supplemented with adenine, leucine, and tryptophan. Diploid isolates that lost the [*FUS3 URA3*] and [*HIS3*] plasmids after nonselective growth were used for tetrad dissection and analysis of segregants from the cross. The **a**-mating (*MATα FUS3*) and α-mating (*MAT***a** *FUS3*) segregants from the cross were screened for the *GPA1E^{21}E^{22}* allele using colony PCR with primers 1223 and 1224 to amplify the 1036–base pair *GPA1* locus, followed by *Bam*HI digestion as described.

C699-331 is a *MAT***a** *fus3Δ6::LEU2 GPA1E^{21}E^{22}* segregant from a cross between strains C699-200 (*MAT***a** *fus3Δ6::LEU2 GPA1*) and C700-29 (*MATα FUS3GPA1 E^{21}E^{22}*). To make this cross, C699-200

Oligo	Sequence (5′ to 3′)	Application
350	ATAGGTGTTGTATTAAGAATG	Forward primer with 1031 for amplification of *STE7* from codon 445
629	CCCAGATGCTGAGTGACG	Forward primer with 881 to confirm *fus3*Δ$^{aa180\text{-}185}$*::COREUK* integration
881	AATCAGCATCCATGTTGGAA	Reverse primer with 629 to confirm *fus3*Δ$^{aa180\text{-}185}$*::COREUK* integration
913	*Sph*I TCAGAGCCCACAGGTCAGCAAAGCGGCATG:C CGCGCGTTGGCCGATTCAT	Composite forward primer for first round of amplification of *fus3*Δ$^{aa180\text{-}185}$*::COREUK*
914	ACATCACCTCTGGCGCCCTGTACCAACGT:TTC GTACGCTGCAGGTCGACG	Composite reverse primer with 913 for first round of amplification of *fus3*Δ$^{aa180\text{-}185}$*::COREUK*
925	TTAGCAAGAATCATTGACGAGTCAGCCGCG-GACAATTCAGAGCCCACAGG	Forward primer for second round of amplification of *fus3*Δ$^{aa180\text{-}185}$*::COREUK*
926	*Nco*I CACGTCCATGGCCCTTGAGTATTTGGCAGAG-GTTAACATCACCTCTGGCG	Reverse primer with 925 for second round of amplification of *fus3*Δ$^{aa180\text{-}185}$*::COREUK*
937	AAGTCGTTACTGGGAGAGGGT	Forward primer for amplification of *FUS3* codons 16–286
938	ATCTATGCCTTTCGGGTTGA	Reverse primer with 937 for amplification of *FUS3* codons 16–286
939	CCAGATGCTGAGTGACGA	Sequencing primer for *FUS3* from codon 107
1031	GCTAACTAGTATTATTCGCAA	Reverse primer with 350 for amplification of *STE7*
1148	AGGAGCCGTAATTTTTGCTT	Reverse primer with 1223
1216	GCAAACAATAGGAGACGAA***t***GTGATCCTTTTCT ACAGAAC:CCGCGCGTTGGCCGATTCAT	Composite forward primer for first round of amplification of *gpa1*Δ$^{aa21\text{-}22}$*::COREUK*
1217	GTTTCTCCAGCTGCAACGATTGCTCGATGACAT CATTGGC:TTCGTACGCTGCAGGTCGAC	Composite reverse primer with 1217
1218	ATATATTAAGGTAGGAAATAATGGGtTGTA-CAGTGAGTACGCAAACAATAGGAGACGAAt	Forward primer for second round of amplification of *gpa1*Δ$^{aa21\text{-}22}$*:: COREUK*
1219	GCACCTAATAGTAACAGTTTTATTTCATTCTTGT-CACGTTGTTTCTCCAGCTGCAACGAT	Reverse primer with 1218 or 1222
1220	HI TGTACAGTGAGTACGCAAACAATAGGAGA-CGAAtcgGATCCTTTTCTACAGAAC***gaagag*** *Bam*HI	Primer annealed with 1221 generates codon subsitutions for *GPA1E*^{21}*E*^{22} with *Bam*HI site
1221	TTTCTCCAGCTGCAACGATTGCTCGATGACAT-CATTGGC***ctcttc***GTTCTGTAGAAAAGG	Primer annealed with 1220 generates codon substitutions for *GPA1E*^{21}*E*^{22} with *Bam*HI site
1222	GAGGTGTATAAATTGATATATTAAGGTAG-GAAATAATGGGtTGTACAGTGAGTACGCAAA	Forward primer with 1219 for extension of annealed oligonucleotides 1220/1221 for the *GPA1E*^{21}*E*^{22} allele with a *Bam*HI site
1223	GCATCTTCGTGTTATTTCAC	Forward primer with 1224 to amplify1036 base pairs of *GPA1* from –396 to codon 213
1224	CTTGGTTCAAGTCCTTGCA	Forward primer with 1224 to amplify1036 base pairs of *GPA1* from –396 to codon 213
1250	TTGTTAGGGTGATGTACACC	Forward primer with 1252 to amplify *MAT*α DNA
1251	CCGCATGGGCAGTTTACC	Forward primer with 1253 to amplify *MAT***a** DNA
1252	CAGCACGGAATATGGGACTA	Reverse primer with 1250 to amplify *MAT*α DNA
1253	TTGTAGTATGGCGGAAAACATAA	Reverse primer with 1251 to amplify *MAT***a** DNA
M13R	CAGGAAACAGCTATGAC	Sequencing primer for pCRBluntII cloned DNA
M13F	TGTAAAACGACGGCCAGT	Sequencing primer for pCRBluntII cloned DNA

Bases in lowercase letters are not homologous to the target DNA. Restriction enzyme recognition sites are underlined and specified above the oligonucleotide sequence. Mutations in codons causing amino acid substitutions are in bold italics.

TABLE 4: Oligonucleotides.

was transformed with YpEE81 [*FUS3 URA3*] to complement the nonmating phenotype of the *fus3*Δ mutant strain, and C700-29 was transformed with pRS313 [*HIS3*] to allow nutritional selection of diploids from mating mixtures on SD supplemented with adenine and tryptophan. Diploid isolates that lost the [*FUS3 URA3*] and [*HIS3*] plasmids after nonselective growth were used for tetrad dissection and analysis of segregants from the cross. Nonmating Leu+ segregants (*fus3*Δ*6::LEU2*) were screened for the *GPA1E*^{21}*E*^{22} allele using colony PCR with primers 1223 and 1224 to amplify the 1036–base pair *GPA1* locus, followed by *Bam*HI digestion as

described. The *MAT* allele of these segregants was distinguished by colony PCR using *MAT*α-specific primers 1250 and 1252 and *MAT***a**-specific primers 1251 and 1253.

Reporter gene assays

The expression of *PRE_3-lacZ* (pGA1706) and *TCS-PRE-lacZ* (pNC343) reporter genes in strains with different *FUS3* and *GPA1* alleles was assessed by measuring β-galactosidase activity. Cultures for these assays were grown to a density of ~(0.8–1.0) × 10^7 cells/ml in –Ura medium to maintain selection for the reporter plasmids. Pheromone (alpha-factor; CHI Scientific, Maynard, MA) was added to 90-μl aliquots of cell culture in microtiter plate wells to final concentrations ranging from 1.0 × 10^{-6} to 1.0 × 10^{-9} M (log scale –6.0 to –9.0). No pheromone reference samples were included. After 90 min of incubation at 30°C, β-galactosidase activity was measured using fluorescein di-β-galactopyranoside (FDG; Marker Gene Technologies, Jacksonville, FL) as substrate. FDG assays in the microtiter plates were carried out as described previously, with activities reported in arbitrary fluorescence units (AU)/min OD_{660} (Hoffman *et al.*, 2002).

Immune blotting conditions for analysis of dual-phosphorylated Fus3 and Kss1

Strains C699-5 (*FUS3*), C699-192 (*fus3A^{180}F^{182}*), and C699-200 (*fus3*Δ) were grown in synthetic complete medium. When cultures reached a cell density of ~1 × 10^7 cells/ml, a 10-ml aliquot was removed to provide an uninduced (t = 0) reference sample. α-Factor was added to a final concentration of 100 nM in the remaining portion of the cultures, and 10-ml aliquots of cells were removed after 30 and 90 min of incubation. Cell lysis, extract preparation, and trichloroacetic acid precipitation were done according to the procedures described by Sabbagh *et al.* (2001). The precipitated protein was suspended in buffer (0. 1 M Tris-HCl, pH 11.0, 3% SDS), boiled for 5 min, and centrifuged for 10 min to remove insoluble aggregates. A 40-μl amount of each sample was mixed with 8 μl of 6× SDS–PAGE loading buffer and boiled for 2 min before being loaded onto 10% SDS–PAGE gels for protein fractionation. Proteins were transferred from the gels to polyvinylidene fluoride membranes for detection of dual-phosphorylated Fus3 and Kss1 by using anti–phospho-p44/42 MAPK rabbit polyclonal antibodies (1:500; Cell Signaling Technologies, Danvers, MA) as primary antibody with horseradish peroxidase (HRP)–conjugated goat anti-rabbit immunoglobulin G (IgG; 1:10,000; Jackson ImmunoResearch, West Grove, PA) as secondary antibody. Antibodies were washed from the membranes by treatment with stripping buffer (Tris-HCl, pH 6.0, SDS, β-mercaptoethanol) and reprobed for glucose-6-phosphate dehydrogenase (G6PDH) as the internal loading control by using rabbit monoclonal anti-G6PDH (1:20,000; Sigma-Aldrich, St. Louis, MO) primary antibody with HRP-conjugated goat anti-rabbit IgG (1:10,000; Jackson ImmunoResearch) as the secondary antibody. Immunoreactive species were detected using ECLplus (GE Healthcare, Amersham, Pittsburgh, PA) and exposing the developed blots to x-ray film. Bands on the scanned x-ray films were quantified using ImageJ software (National Institutes of Health, Bethesda, MD).

Time-lapse imaging to follow pheromone gradient tracking, morphology, and G1 arrest

These analyses were done in 5–50 nM pheromone gradients using a microfluidic device and methods for cell culturing, cell loading, and gradient generation as described in the supplement to Hao *et al.* (2008). Differential interference contrast (DIC) images of cells from four to six different fields that span the entire gradient were captured at 5-min intervals for a 5-h time course.

Microscopy was performed with a Nikon Ti-E inverted microscope using a Plan Fluor ELWD 40×/0.6 Nikon objective and a Photometrics CoolSNAP HQ2 Monochrome camera. Acquisition was performed with MetaMorph software (Molecular Devices, Sunnyvale, CA). Image processing and cell scoring were aided by use of ImageJ software.

The morphological categories scored after 5 h of growth in the pheromone gradient are illustrated by micrographs in Figure 2D. Unbudded cells (whether vegetative, shmoo, or hyperelongated) in each of the fields were also scored to assess the percentage of G1 cells in the population. The distinction between mothers with large buds (G2/M) versus unbudded mother–daughter pairs (G1) was aided by time-lapse imaging. Cells were scored as G1 if a bud emerged from either within the next two 5-min intervals.

Gradient tracking was quantified in cells 4.5 h after growth in the pheromone gradient. The angle between the cell center and the furthest point of the leading edge was measured using the straight-line tool in FIJI (fiji.sc/Fiji; Schindelin *et al.*, 2012). The measured angles were then normalized in relation to the direction of the gradient and the chamber orientation. A histogram of the angles was generated using Matlab (MathWorks, Natick, MA). The histogram was normalized to represent the percentage of cells in each bin and plotted as a figure using the Polar function in Matlab.

P_{GAL1}STE5-CTM morphology and G1 assays

Cells were cultured for these assays in synthetic complete medium with 2% raffinose as the carbon source. Cells were loaded into the microfluidic chamber as described in the supplement to Hao *et al.* (2008) and exposed to medium with uniform 2% galactose to induce expression of Ste5-CTM from the galactose-inducible *GAL1,10* promoter. DIC images of cells from four to six different fields were captured at 10-min intervals for a 12-h time course. Microscopy was performed as before except using a 60× Plan Apo 1. 4 Nikon objective. Scoring of morphology before the switch to galactose and after 12 h of growth in galactose was done as described, and the categories are illustrated by micrographs in Figure 5A. Vegetative, shmoo, and hyperelongated cells that are unbudded were also scored to assess the percentage of G1 cells in the population as described earlier.

Pheromone dose-response morphology and G1 assays

Strains were exposed to uniform pheromone for dose-response comparisons. In these experiments, 50-ml cultures of each strain were grown in yeast extract/peptone/dextrose medium to ~2. 5 × 10^6 cells/ml. The cultures were divided into 4-ml aliquots in culture tubes. Pheromone was added to each tube to final concentration ranging from 3.16 × 10^{-7} to 3.16 × 10^{-9} M (log scale –6.5 to –8.5). After 5 h of incubation at 30°C, a 250-μl sample was removed to an Eppendorf tube, cells were sonicated mildly to disperse clumps, and formaldehyde solution was added a final concentration of 2% to fix the cells. Cell morphology was scored on the fixed cell suspensions with a hemocytometer and an aus Jena Laboval microscope with a 40×/0.65 objective. Unbudded cells were also scored to assess the G1 population as described earlier.

ACKNOWLEDGMENTS

We thank H. Dohlman, D. Lew, J. Kelley, and J. Purvis for stimulating discussions and comments on the manuscript. This work was supported by National Institutes of Health Grants GM079271, GM084071, and GM114136 (T.C.E. and B.E.).

REFERENCES

Akada R, Murakane T, Nishizawa Y (2000). DNA extraction method for screening yeast clones by PCR. Biotechniques 28, 668–670, 672, 674.

Alani E, Cao L, Kleckner N (1987). A method for gene disruption that allows repeated use of URA3 selection in the construction of multiply disrupted yeast strains. Genetics 116, 541–545.

Amberg DC, Burke DJ, Strathern JN (2005). Methods in Yeast Genetics, Cold Spring Harbor, NY: Cold Spring Harbor Laboratory Press.

Bao MZ, Schwartz MA, Cantin GT, Yates JR 3rd, Madhani HD (2004). Pheromone-dependent destruction of the Tec1 transcription factor is required for MAP kinase signaling specificity in yeast. Cell 119, 991–1000.

Bardwell L, Cook JG, Voora D, Baggott DM, Martinez AR, Thorner J (1998a). Repression of yeast Ste12 transcription factor by direct binding of unphosphorylated Kss1 MAPK and its regulation by the Ste7 MEK. Genes Dev 12, 2887–2898.

Bardwell L, Cook JG, Zhu-Shimoni JX, Voora D, Thorner J (1998b). Differential regulation of transcription: repression by unactivated mitogen-activated protein kinase Kss1 requires the Dig1 and Dig2 proteins. Proc Natl Acad Sci USA 95, 15400–15405.

Baur M, Esch RK, Errede B (1997). Cooperative binding interactions required for function of the Ty1 sterile responsive element. Mol Cell Biol 17, 4330–4337.

Blondel M, Alepuz PM, Huang LS, Shaham S, Ammerer G, Peter M (1999). Nuclear export of Far1p in response to pheromones requires the export receptor Msn5p/Ste21p. Genes Dev 13, 2284–2300.

Boeke JD, LaCroute F, Fink GR (1994). A positive selection for mutants lacking orotidine-5′phosphate decarboxylase activity in yeast. Mol Gen Genet 197, 354–356.

Breitkreutz A, Boucher L, Breitkreutz BJ, Sultan M, Jurisica I, Tyers M (2003). Phenotypic and transcriptional plasticity directed by a yeast mitogen-activated protein kinase network. Genetics 165, 997–1015.

Breitkreutz A, Boucher L, Tyers M (2001). MAPK specificity in the yeast pheromone response independent of transcriptional activation. Curr Biol 11, 1266–1271.

Breitkreutz A, Tyers M (2002). MAPK signaling specificity: it takes two to tango. Trends Cell Biol 12, 254–257.

Bruckner S, Kohler T, Braus GH, Heise B, Bolte M, Mosch HU (2004). Differential regulation of Tec1 by Fus3 and Kss1 confers signaling specificity in yeast development. Curr Genet 46, 331–342.

Butty AC, Pryciak PM, Huang LS, Herskowitz I, Peter M (1998). The role of Far1p in linking the heterotrimeric G protein to polarity establishment proteins during yeast mating. Science 282, 1511–1516.

Chang CF, D'Souza WN, Ch'en IL, Pages G, Pouyssegur J, Hedrick SM (2012). Polar opposites: Erk direction of CD4 T cell subsets. J Immunol 189, 721–731.

Chou S, Huang L, Liu H (2004). Fus3-regulated Tec1 degradation through SCFCdc4 determines MAPK signaling specificity during mating in yeast. Cell 119, 981–990.

Chou S, Lane S, Liu H (2006). Regulation of mating and filamentation genes by two distinct Ste12 complexes in Saccharomyces cerevisiae. Mol Cell Biol 26, 4794–4805.

Cook JG, Bardwell L, Kron SJ, Thorner J (1996). Two novel targets of the MAP kinase Kss1 are negative regulators of invasive growth in the yeast Saccharomyces cerevisiae. Genes Dev 10, 2831–2848.

Cook JG, Bardwell L, Thorner J (1997). Inhibitory and activating functions for MAPK Kss1 in the S. cerevisiae filamentous-growth signalling pathway. Nature 390, 85–88.

Corson LB, Yamanaka Y, Lai KM, Rossant J (2003). Spatial and temporal patterns of ERK signaling during mouse embryogenesis. Development 130, 4527–4537.

Dohlman HG, Thorner JW (2001). Regulation of G protein-initiated signal transduction in yeast: paradigms and principles. Annu Rev Biochem 70, 703–754.

Elion EA, Brill JA, Fink GR (1991). FUS3 represses CLN1 and CLN2 and in concert with KSS1 promotes signal transduction. Proc Natl Acad Sci USA 88, 9392–9396.

Elion EA, Grisafi PL, Fink GR (1990). FUS3 encodes a cdc2+/CDC28-related kinase required for the transition from mitosis into conjugation. Cell 60, 649–664.

Erdman S, Snyder M (2001). A filamentous growth response mediated by the yeast mating pathway. Genetics 159, 919–928.

Esch RK, Errede B (2002). Pheromone induction promotes Ste11 degradation through a MAPK feedback and ubiquitin-dependent mechanism. Proc Natl Acad Sci USA 99, 9160–9165.

Esch RK, Wang Y, Errede B (2006). Pheromone-induced degradation of Ste12 contributes to signal attenuation and the specificity of developmental fate. Eukaryot Cell 5, 2147–2160.

Farley FW, Satterberg B, Goldsmith EJ, Elion EA (1999). Relative dependence of different outputs of the Saccharomyces cerevisiae pheromone response pathway on the MAP kinase Fus3p. Genetics 151, 1425–1444.

Fischer AM, Katayama CD, Pages G, Pouyssegur J, Hedrick SM (2005). The role of erk1 and erk2 in multiple stages of T cell development. Immunity 23, 431–443.

Gartner A, Nasmyth K, Ammerer G (1992). Signal transduction in Saccharomyces cerevisiae requires tyrosine and threonine phosphorylation of FUS3 and KSS1. Genes Dev 6, 1280–1292.

Guarente L, Lalonde B, Gifford P, Alani E (1984). Distinctly regulated tandem upstream activation sites mediate catabolite repression of the CYC1 gene of S. cerevisiae. Cell 36, 503–511.

Hao N, Nayak S, Behar M, Shanks RH, Nagiec MJ, Errede B, Hasty J, Elston TC, Dohlman HG (2008). Regulation of cell signaling dynamics by the protein kinase-scaffold Ste5. Mol Cell 30, 649–656.

Hao N, Yildirim N, Nagiec MJ, Parnell SC, Errede B, Dohlman HG, Elston TC (2012). Combined computational and experimental analysis reveals mitogen-activated protein kinase-mediated feedback phosphorylation as a mechanism for signaling specificity. Mol Biol Cell 23, 3899–3910.

He Y, Staser K, Rhodes SD, Liu Y, Wu X, Park SJ, Yuan J, Yang X, Li X, Jiang L, *et al*. (2011). Erk1 positively regulates osteoclast differentiation and bone resorptive activity. PLoS One 6, e24780.

Hoffman GA, Garrison TR, Dohlman HG (2002). Analysis of RGS proteins in Saccharomyces cerevisiae. Methods Enzymol 344, 617–631.

Johnston M, Davis RW (1984). Sequences that regulate the divergent GAL1-GAL10 promoter in Saccharomyces cerevisiae. Mol Cell Biol 4, 1440–1448.

Kelley JB, Dixit G, Sheetz JB, Venkatapurapu SP, Elston TC, Dohlman HG (2015). RGS proteins and septins cooperate to promote chemotropism by regulating polar cap mobility. Curr Biol 25, 275–285.

Lawrence MC, McGlynn K, Shao C, Duan L, Naziruddin B, Levy MF, Cobb MH (2008). Chromatin-bound mitogen-activated protein kinases transmit dynamic signals in transcription complexes in beta-cells. Proc Natl Acad Sci USA 105, 13315–13320.

Leeuw T, Wu C, Schrag JD, Whiteway M, Thomas DY, Leberer E (1998). Interaction of a G-protein beta-subunit with a conserved sequence in Ste20/PAK family protein kinases. Nature 391, 191–195.

Liu H, Styles CA, Fink GR (1993). Elements of the yeast pheromone response pathway required for filamentous growth of diploids. Science 262, 1741–1744.

Madhani HD, Styles CA, Fink GR (1997). MAP kinases with distinct inhibitory functions impart signaling specificity during yeast differentiation. Cell 91, 673–684.

Maleri S, Ge Q, Hackett EA, Wang Y, Dohlman HG, Errede B (2004). Persistent activation by constitutive ste7 promotes kss1-mediated invasive growth but fails to support fus3-dependent mating in yeast. Mol Cell Biol 24, 9221–9238.

Matheos D, Metodiev M, Muller E, Stone D, Rose MD (2004). Pheromone-induced polarization is dependent on the Fus3p MAPK acting through the formin Bni1p. J Cell Biol 165, 99–109.

Metodiev MV, Matheos D, Rose MD, Stone DE (2002). Regulation of MAPK function by direct interaction with the mating-specific Galpha in yeast. Science 296, 1483–1486.

Nguyen HN, Hadwiger JA (2009). The Galpha4 G protein subunit interacts with the MAP kinase ERK2 using a D-motif that regulates developmental morphogenesis in Dictyostelium. Dev Biol 335, 385–395.

Palecek SP, Parikh AS, Kron SJ (2002). Sensing, signalling and integrating physical processes during Saccharomyces cerevisiae invasive and filamentous growth. Microbiology 148, 893–907.

Paliwal S, Iglesias PA, Campbell K, Hilioti Z, Groisman A, Levchenko A (2007). MAPK-mediated bimodal gene expression and adaptive gradient sensing in yeast. Nature 446, 46–51.

Peter M, Gartner A, Horecka J, Ammerer G, Herskowitz I (1993). FAR1 links the signal transduction pathway to the cell cycle machinery in yeast. Cell 73, 747–760.

Pryciak PM, Huntress FA (1998). Membrane recruitment of the kinase cascade scaffold protein Ste5 by the Gbetagamma complex underlies activation of the yeast pheromone response pathway. Genes Dev 12, 2684–2697.

Raisley B, Nguyen HN, Hadwiger JA (2010). G{alpha}5 subunit-mediated signalling requires a D-motif and the MAPK ERK1 in Dictyostelium. Microbiology 156, 789–797.

Reneke JE, Blumer KJ, Courchesne WE, Thorner J (1988). The carboxy-terminal segment of the yeast alpha-factor receptor is a regulatory domain. Cell 55, 221–234.
Rhodes N, Company M, Errede B (1990). A yeast-Escherichia coli shuttle vector containing the M13 origin of replication. Plasmid 23, 159–162.
Roberts CJ, Nelson B, Marton MJ, Stoughton R, Meyer MR, Bennett HA, He YD, Dai H, Walker WL, Hughes TR, *et al.* (2000). Signaling and circuitry of multiple MAPK pathways revealed by a matrix of global gene expression profiles. Science 287, 873–880.
Roberts RL, Fink GR (1994). Elements of a single MAP kinase cascade in Saccharomyces cerevisiae mediate two developmental programs in the same cell type: mating and invasive growth. Genes Dev 8, 2974–2985.
Rodriguez J, Crespo P (2011). Working without kinase activity: phosphotransfer-independent functions of extracellular signal-regulated kinases. Sci Signal 4, re3.
Rothstein RJ (1983). One-step gene disruption in yeast. Methods Enzymol 101, 202–211.
Sabbagh W Jr, Flatauer LJ, Bardwell AJ, Bardwell L (2001). Specificity of MAP kinase signaling in yeast differentiation involves transient versus sustained MAPK activation. Mol Cell 8, 683–691.
Sarbassov DD, Jones LG, Peterson CA (1997). Extracellular signal-regulated kinase-1 and -2 respond differently to mitogenic and differentiative signaling pathways in myoblasts. Mol Endocrinol 11, 2038–2047.
Schindelin J, Arganda-Carreras I, Frise E, Kaynig V, Longair M, Pietzsch T, Preibisch S, Rueden C, Saalfeld S, Schmid B, *et al.* (2012). Fiji: an open-source platform for biological-image analysis. Nat Methods 9, 676–682.
Schrick K, Garvik B, Hartwell LH (1997). Mating in Saccharomyces cerevisiae: the role of the pheromone signal transduction pathway in the chemotropic response to pheromone. Genetics 147, 19–32.
Segall JE (1993). Polarization of yeast cells in spatial gradients of alpha mating factor. Proc Natl Acad Sci USA 90, 8332–8336.
Shilo BZ (2003). Signaling by the Drosophila epidermal growth factor receptor pathway during development. Exp Cell Res 284, 140–149.
Shilo BZ (2005). Regulating the dynamics of EGF receptor signaling in space and time. Development 132, 4017–4027.
Shimada Y, Gulli MP, Peter M (2000). Nuclear sequestration of the exchange factor Cdc24 by Far1 regulates cell polarity during yeast mating. Nat Cell Biol 2, 117–124.
Shin S, Dimitri CA, Yoon SO, Dowdle W, Blenis J (2010). ERK2 but not ERK1 induces epithelial-to-mesenchymal transformation via DEF motif-dependent signaling events. Mol Cell 38, 114–127.
Sikorski RS, Hieter P (1989). A system of shuttle vectors and yeast host strains designed for efficient manipulation of DNA in Saccharomyces cerevisiae. Genetics 122, 19–27.
Storici F, Resnick MA (2006). The delitto perfetto approach to in vivo site-directed mutagenesis and chromosome rearrangements with synthetic oligonucleotides in yeast. Methods Enzymol 409, 329–345.
Tedford K, Kim S, Sa D, Stevens K, Tyers M (1997). Regulation of the mating pheromone and invasive growth responses in yeast by two MAP kinase substrates. Curr Biol 7, 228–238.
Truckses DM, Garrenton LS, Thorner J (2004). Jekyll and Hyde in the microbial world. Science 306, 1509–1511.
van Drogen F, O'Rourke SM, Stucke VM, Jaquenoud M, Neiman AM, Peter M (2000). Phosphorylation of the MEKK Ste11p by the PAK-like kinase Ste20p is required for MAP kinase signaling in vivo. Curr Biol 10, 630–639.
Wang Y, Dohlman HG (2006). Pheromone-regulated sumoylation of transcription factors that mediate the invasive to mating developmental switch in yeast. J Biol Chem 281, 1964–1969.
Whiteway MS, Wu C, Leeuw T, Clark K, Fourest-Lieuvin A, Thomas DY, Leberer E (1995). Association of the yeast pheromone response G protein beta gamma subunits with the MAP kinase scaffold Ste5p. Science 269, 1572–1575.
Wu C, Whiteway M, Thomas DY, Leberer E (1995). Molecular characterization of Ste20p, a potential mitogen-activated protein or extracellular signal-regulated kinase kinase (MEK) kinase kinase from Saccharomyces cerevisiae. J Biol Chem 270, 15984–15992.